國立彰化師範大學物理研究所

碩士論文

指導教授：郭艷光教授

氮化銦鎵與磷化鋁鎵銦面射型半導體雷射光學特性之研究

A Study of the Optical Properties of InGaN and AlGaInP Vertical-Cavity Surface-Emitting Lasers

研究生：黃旭晴撰

中華民國九十年七月

國立彰化師範大學物理研究所

碩士論文

研究生：黃旭晴

氮化銦鎵與磷化鋁鎵銦面射型半導體雷射光學特性之研究

A Study of the Optical Properties of InGaN and AlGaInP Vertical-Cavity Surface-Emitting Lasers

本論文業經審查及口試合格特此證明

論文考試委員會主席____________

委員：____________　____________

指導教授：郭艷光教授____________

所長：張惠博主任____________

中華民國九十年七月

授權書
(博碩士論文)

本授權書所授權之論文為本人在 彰化師範 大學(學院) 物理 系所 ______ 組 89 學年度第 2 學期取得 碩 士學之論文。

論文名稱：氮化銦鎵與磷化鋁鎵銦面射型半導體雷射光學特性之研究

□同意　□不同意

本人具有著作財產權之論文全文資料，授予行政院國家科學委員會科學技術資料中心、國家圖書館及本人畢業學校圖書館，得不限地域、時間與次數以微縮、光碟或數位化等各種方式重製後散布發行或上載網路。本論文為本人向經濟部智慧財產局申請專利的附件之一，請將全文資料延後兩年後再公開。(請註明文號：　　　　　　　　　　　　)

□同意　□不同意

本人具有著作財產權之論文全文資料，授予教育部指定送繳之圖書館及本人畢業學校圖書館，為學術研究之目的以各種方法重製，或為上述目的再授權他人以各種方法重製，不限地域與時間，惟每人一份為限。

上述授權內容均無須訂立讓與及授權契約書。依本授權之發行權為非專屬性發行權利。依本授權所為之收錄、重製、發行及學術研究利用為無償。上述同意與不同意之欄位若未鉤選，本人同意視同授權。

指導教授姓名： 郭艷光

研究生簽名：黃旭晴　　學號：8822212
(親筆正楷)　　(務必填寫)

日期：民國 90 年 6 月 30 日

---

1. 本授權書請以黑筆撰寫並影印裝訂於書名頁之次頁。
2. 授權第一項者，請再交論文一本予畢業學校承辦人員或逕寄 106-36 台北市和平路二段 106 路 1702 室國科會科學扳術資料中心王淑貞。（電話 02-27377746）
3. 本授權書已於民國 85 年 4 月 10 日送請內政部著作權委員會(現為經濟部智慧財產局)修正定稿。
4. 本案依據教育部國家圖書館 85.4.19 台(85)圖編字第 712 號函辦理。

To my dad, my mom, Kevin, Jason, and all my friends.

Acknowledgment

First of all, I must offer my heartfelt appreciation to my academic advisor, Professor Yen-Kuang Kuo, for his diligent help in these two years. He is not only my adored teacher in the laboratory but also our kind member of Quantum Rock in Pop Music Club. He always teaches me great lessons and trains me to be a mature boy and to be growing-up.

I ought to thank Professor Jiann Lin for providing me the software key of PICS3D simulation program to accomplish my thesis and serving as my thesis committee member. Besides, I would like to thank Doctor Man-Fang Huang for being the chairman of my thesis committee.

I am much grateful to Yuni Chang, my best partner, for her support not only on my studies in school but also my daily life. She taught me what I am and deal with me as I am the king of the world. Thanks for her being with me and her helping me to go through all the difficulties. Your sincerity really inspires me a lot.

Thanks for Kuo-Kai Horng, Ya-Lien Huang, Jih-Yuan Chang, Wen-Wei Lin, Yi-An Chang, Chih-Kang Chang, Horng-Min Chen and Chia-Ching Lin, my best friends. They always support me, showing their greatest concerns for me. I know, we will be good friends for a long long time to come.

I am thankful to the boss of Gu-Xiang Foodstuff for that he always supplies the foods for me to burn the midnight oil. I am also thankful to

Jun-Hong Xu, a student in institute of mathematics, for that he always urges me again and again to finish my thesis.

Life is a long lesson, for seeking for the true self and making me a really myself. Thanks to all the people I have ever known in Chang-Hua. You light up my life.

An enlightened man had but one duty --- to seek the way to himself, to reach inner certainty, to grope his way forward, no matter where it led.

~ Hermann Hesse ~

Table of Contents

List of Figures……………………………………………………… VIII

List of Tables…………………………………………………………XII

Abstract……………………………………………………………… XIV

Chapter 1. Introduction…………………………………………… 1

1.1 Introduction to AlGaInP Based Diodes………………………2

1.2 Introduction to AlGaInN Based Diodes……………………… 7

1.3 Introduction to VCSEL……………………………………… 11

Chapter 2. The Electrical and Optical Properties of AlGaInP Based Multi-Quantum Well Vertical Cavity Surface Emitting Laser Diodes………………………………… 17

2.1 Characteristics of AlGaInP Lasers and POF………………… 18

2.2 Structures of the Laser Diodes Under Study………………… 20

2.3 The Electrical and Optical Properties of the VCSELs……… 23

2.4 Discussion……………………………………………………… 42

Chapter 3. Numerical Study on an Electrically Pumped 440-nm InGaN Vertical-Cavity Surface-Emitting Laser……………… 47

3.1 Characteristics of InGaN MQW Lasers………………………… 49

3.2 Structures of the Diodes……………………………………… 52

3.3 The Electrical and Optical Properties of the VCSELs……… 58

3.4 Discussion……………………………………………………… 71

Chapter 4. Conclusion……………………………………………… 75

Appendix A. User guides of PICS3D…….......……………………... 77
Appendix B. Trouble Shooting......……………….............................….. 82

List of Figures

Fig. 1.1 Lattice constants and bandgap energy of variant materials..…..5

Fig. 1.2 Energy levels diagram in quantum well……………….……..5

Fig. 1.3 Refractive index of AlGaInP from 3.0 (AlInP) to 3.2 (GaInP)..6

Fig. 1.4 Structure of AlGaInN based LED and LD……………….…… 10

Fig. 1.5 High quality laser diode with E-LOG substrate grown by Nichia Inc..........…………………………………………………......... 10

Fig. 1.6 Paths of light crossing the DBR……….…………………… 13

Fig. 2.1 Transmission loss spectra of PMMA-d8 core POF..........……19

Fig. 2.2 Structures of the two VCSEL devices with different DBR under study: (a) AlGaInP, (b) AlGaAs……………………………… 22

Fig. 2.3 (a) Reflectivity spectra for different pairs of DBR (AlGaInP). (b) Reflectivity spectra for different pairs of DBR (AlGaAs).. 29

Fig. 2.4 (a) Log of electron concentration when the injection current is 11.19mA (AlGaInP). (b) Log of electron concentration when the injection current is 11.19mA (AlGaAs)………………….. 30

Fig. 2.5 (a) Log of hole concentration when the injection current is 11.19mA (AlGaInP). (b) Log of hole concentration when the injection current is 11.19mA (AlGaAs)…………………….... 31

Fig. 2.6 Stimulated recombination rate in the active region.………..…32

Fig. 2.7 L-I curves of these two diodes..…………………………....32

Fig. 2.8 (a) I-V curves of the diode (AlGaInP). (b) I-V curves of the diode (AlGaAs)……………………………………………33

Fig. 2.9 (a) Power transformation curves of the diode (AlGaInP). (b)

Power transformation curves of the diode (AlGaAs)…..…… 34

Fig. 2.10 (a) L-I curves of the diode with core radius of 10 μm and 5μm (AlGaInP). (b) L-I curves of the diode with core radius of 10 μm and 5μm (AlGaAs)……………………………………… 35

Fig. 2.11 (a) I-V curves of the diode of variant core radius (AlGaInP). (b) I-V curves of the diode of variant core radius (AlGaAs)…36

Fig. 2.12 (a) Power transformation curves of the diode with variant core radius (AlGaInP). (b) Power transformation curves of the diode with variant core radius (AlGaAs)…………………………... 37

Fig. 2.13 (a) Structure of the VCSEL devices with current-spreading (AlGaInP). (b) Structure of the VCSEL devices with current-spreading (AlGaAs)………………………………..... 38

Fig. 2.14 (a) L-I curves of the devices with gain-guiding structures (AlGaInP). (b) L-I curves of the devices with gain-guiding structures (AlGaAs)………………………………………….. 39

Fig. 2.15 (a) I-V curves of the devices with gain-guiding structures (AlGaInP). (b) I-V curves of the devices with gain-guiding structures (AlGaAs)………………………………………….. 40

Fig. 2.16 (a) Power transformation curves of the diode with gain-guiding structures (AlGaInP). (b) Power transformation curves of the diode with gain-guiding structures (AlGaAs)………………...41

Fig. 3.1 Relation between indium composition and the peak wavelength of GaInN bulk...……………..51

Fig. 3.2 Wavelength as a function of well width when the composition of indium in well and barrier are 0.14 and 0.01.......………....51

Fig. 3.3 Reflectivity spectra of 15 pairs of GaN/$Al_{0.27}Ga_{0.73}N$ DBR….54

Fig. 3.4 Reflectivity Spectra of 15 pairs of GaN/Al0.27Ga0.73N DBR simulated by PICS3D simulation program......…..…………..54

Fig. 3.5 Cross-sectional structure of the blue InGaN VCSEL under study.. 55

Fig. 3.6 Reflectivity spectra of the GaN/$Al_{0.27}Ga_{0.73}N$ DBR when the pair number of the DBR is equal to 10, 20, 30, 40, 50 and 60.. 61

Fig. 3.7 L-I curve of the InGaN VCSEL under study at room temperature.. 61

Fig. 3.8 (a) Mode spectrum when the injection current is at 33.9 mA. (b) Mode spectrum when the injection current is at 41.4 mA.......62

Fig. 3.9 Side mode suppression ratio as a function of the injection current.. 63

Fig. 3.10 (a) Distribution of the electron concentrations obtained at an injection current of 41.4 mA. The inset of figure is the magnified view of the electron and hole concentrations near the MQW. (b) Distribution of the hole concentrations obtained at an injection current of 41.4 mA. The inset of figure is the magnified view of the electron and hole concentrations near the MQW.. 64

Fig. 3.11 Diagram of the stimulated recombination rates.......................65

Fig. 3.12 Wave intensity diagram.. 65

Fig. 3.13 (a) Threshold current with different numbers of quantum wells. (b) Current to light output conversion with different numbers of quantum wells..66

Fig. 3.14 Laser output power as a function of current for the devices with variant diameter.. 67

Fig. 3.15 Laser output power as functions of electric power with variance device diameters..67

Fig. 3.16 L-I Curve of the InGaN VCSEL with 40-pairs of p-DBR under

Study.....……………………..……………….……………68

Fig. 3.17 (a) Threshold current with different numbers of quantum wells. (b) Current to light output conversion with different numbers of quantum wells………………………………………….…69

Fig. 3.18 I-V curves of devices with variant numbers of quantum wells ……………………………………………………………..70

Fig. 3.19 Power transformation curves of the diode with variant numbers of quantum wells.........………………………...……………70

List of Tables

Table 1.1. Comparison between Al_2O_3 and SiC substrates. 8

中文摘要

我們利用 PICS3D 商用模擬軟體來模擬以磷化鋁鎵銦與氮化鋁鎵銦為材料所成長的面射型半導體雷射，並設計不同的結構以比較其雷射的操作效能。

在磷化鋁鎵銦的面射型雷射方面，我們將波長鎖定在 670nm，以磷化鋁鎵銦做雷射的活性層，然後分別使用砷化物與磷化物來做為雷射的 DBR，模擬的結果顯示以砷化物所做的 DBR 在同樣的對數之下會有比較高的反射率，而且以砷化物作為 DBR 的面射型雷射其運作時的下限電流會比較小，而且在同一電流之下，雷射的輸出功率也會比較大，我們並以此為出發點，繼而探討不同的 gain-guiding 結構對雷射效能與輸出功率的影響。模擬所得的結果是當使用 gain-guiding 結構時，雖然可以降低雷射的下限電流，但是也會相對的降低雷射操作時的 slope efficiency。

在氮化鋁鎵銦的面射型雷射方面，我們以氮化銦鎵做雷射的活性層，然後用氮化鋁鎵來做為雷射的 DBR，將雷射的輸出波長鎖定在 440nm，探討不同對數的 DBR 與 gain-guiding 結構對雷射操作效能的影響，模擬的結果顯示當 DBR 的對數為 40-50 對時會有最小的下限電流，而且使用 gain-guiding 結構也可以使雷射的下限電流降低，但與磷化鋁鎵銦的面射型雷射相反的是氮化鋁鎵銦的面射型雷射使用 gain-guiding 結構以後的 slope efficiency 也會提高。

Abstract

In this thesis, we investigate the AlGaInP and AlGaInN based vertical-cavity surface-emitting laser (VCSEL) with PICS3D (Photonic Integrated Circuit Simulator in 3D) commercial simulation program. Besides, we design different structures to compare the operating efficiency of laser performance.

For the AlGaInP based muti-quantum well (MQW) VCSEL emitting at 670 nm, we take the AlGaAs and AlGaInP as the materials of distributed Bragger reflector (DBR). The simulation results show that the reflectivity spectrum of VCSEL with AlGaAs DBR is superior to AlGaInP one when the pair numbers of the DBR are the same. Besides, this kind of VCSEL will result in lower threshold current and higher laser output power at the same current injection. Afterwards, we study the laser performance and laser output power with gain-guiding structure. Finally, the VCSEL with gain-guiding structure will lower the threshold current of a VCSEL but result in lowering the slope efficiency of operating efficiency of laser performance.

For the AlGaInN based MQW VCSEL emitting at 440 nm, we take the InGaN as the materials of MQW and the AlGaN as the DBR of the VCSEL. In this chapter, we investigate the laser performance with different DBR pairs. In addition, the gain-guiding structure is also discussed. The simulation results show that when the DBR pairs of n-DBR and p-DBR are defined as 50 and 40 respectively, we obtain the lowest threshold current. By introducing the gain-guiding structure, we obtain the same results too.

However, the slope efficiency of the AlGaInN based VCSEL will increase with gain-guiding structure, which is in contrast with that of the AlGaInP based VCSEL.

Chapter 1. Introduction

Semiconductor materials improve our daily life very much. The importance of III-phosphide and III-nitride semiconductor laser is increasing due to its application in optical fiber communication, data storage, traffic light, and so on. In the future, we can anticipate that the semiconductor material plays an important role in human life.

1.1 Introduction to AlGaInP Based Diodes

The quaternary $Al_xGa_yIn_{1-x-y}P$ alloy is made up of AlP, GaP and InP. It has been widely used in light emitting diode (LED) and laser diode (LD). AlP, GaP, and InP have their own band gap. As shown in Fig. 1.1, at room temperature, the band gaps of AlP, GaP, and InP are 2.45 eV, 2.26 eV, and 1.35 eV, respectively, and their corresponding characteristic wavelengths are 510m, 550nm, and 920nm. It is thus clear that we can generate numerous percentage of each material to achieve different emitting wavelength. Generally, the AlGaInP materials are grown on GaAs substrates [1]. The lattice constant of AlP is about 5.46 Å, and that of GaP is about 5.45 Å, almost the same with that of AlP. However, the lattice constant of InP is 5.86 Å, and that of GaAs substrate is 5.65 Å [2]. By considering about lattice match when grown on GaAs substrate, the composition of InP must be fixed at fifty percent and the other fifty percent can be modulated by AlP and GaP arbitrarily. The representation of the compounds can be expressed as $(Al_xGa_{1-x})_{0.5}In_{0.5}P$ and the emitting wavelength is ranging from green to red light region.

Another problem is the light emitting efficiency of the material. For $(Al_xGa_{1-x})_{0.5}In_{0.5}P$, as long as the variable x is lager than about 0.53, it becomes an indirect bandgap material. As a consequence, it results in poor light emitting efficiency. In fact, when the variable x is larger than 0.3, the efficiency of light output is gradually decreasing. Therefore, we cannot grow high power and high brightness optical diodes when the aluminum composition is high. In addition, aluminum is easy to get oxidized, and the

oxidized aluminum will increase the defects in the films and hence decrease the light emitting efficiency. Hence, we would rather lower the composition of aluminum when growing diodes. These factors limit the development of $(Al_xGa_{1-x})_{0.5}In_{0.5}P$ materials in short wavelength. There are two ways can be utilized to overcome these difficulties, one is to use the quantum well structure, and the other is to introduce the strain effect [3-6].

If we grow quantum well structure in the active region, the lower energy levels in conduction band and valance band will be separated from each other. The continuous energy band then breaks into discontinuous energy levels, and the first energy level in conduction band will be higher than the bottom of the band, similarly, the first energy level in valance band will be lower than the top of the band, as shown in the Fig. 1.2. There are three advantages after inducing this effect. Firstly, we can get narrower full width at half maximum (FWHM) of the emission spectrum. Secondly, it may help increase the overlap probability of electron and photon in space, and hence raise the light emitting efficiency. Finally, it results in shorter emission wavelength with equal aluminum composition. From Eq. (1):

$$E_g(x)=1.91+0.61x \text{ (eV)}, \quad (1)$$

bandgap energy of the $(Al_xGa_{1-x})_{0.5}InP$ is 2.093 eV when x is equal to 0.3 and the emitting wavelength is about 590 nm. Furthermore, the emitting wavelength will become about 570 nm if we take the quantum well structure into consideration in proper well width and depth. Since the effective mass of the holes is larger than that of the electrons, the split in valance band of energy levels is not as obvious as in conduction band. Therefore, the emitting wavelength is dominated by conduction band [7].

Unfortunately, the quantum well structure brings us short emitting wavelength but results in current overflow. For the AlGaInP based semiconductor laser, emitting at shorter wavelength with shorter band offset, electrons flows into cladding layers easily. The overflow electrons will not contribute to light emitting but cause thermal energy. It will thus reduce the efficiency of light emitting. In contrast, if we take strain effect into quantum well structure, we will improve the problems of current overflow [8-9]. In addition, the strain effect will increase the spontaneous emission rates of electrons and bring us higher light emitting efficiency in quantum well.

As shown in Fig. 1.3, the refractive index of AlGaInP is tunable only from 3.0 (AlInP) to 3.2 (GaInP). It is of disadvantage for designing distributed Bragger reflectors (DBR). It is one of the major limitations for developing DBR of AlGaInP based materials. For red spectral region vertical-cavity surface-emitting laser (VCSEL), although we can grow the DBR with AlGaInP materials, AlGaAs materials are used in general. This is mainly due to the fact that the refractive index difference between AlAs (2.92) and GaAs (3.6) is larger than that of AlGaInP based DBR. In other words, when compared with AlGaInP materials, we can grow DBR by using AlGaAs epitaxial layers to obtain higher reflectivity if the pair numbers are the same.

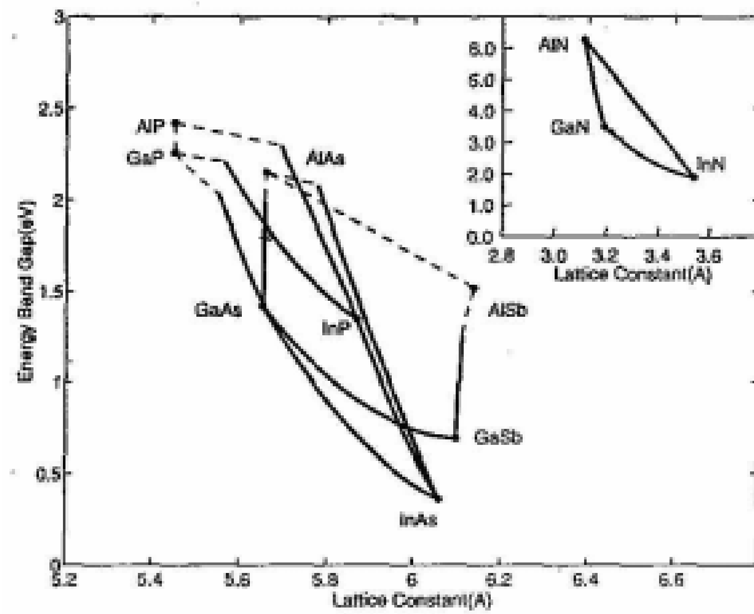

Fig. 1.1 Lattice constants and bandgap energy of variant materials.

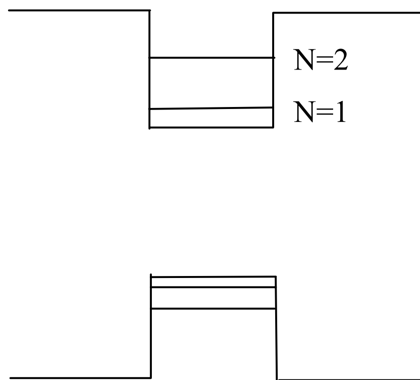

Fig. 1.2 Energy level diagram in quantum well.

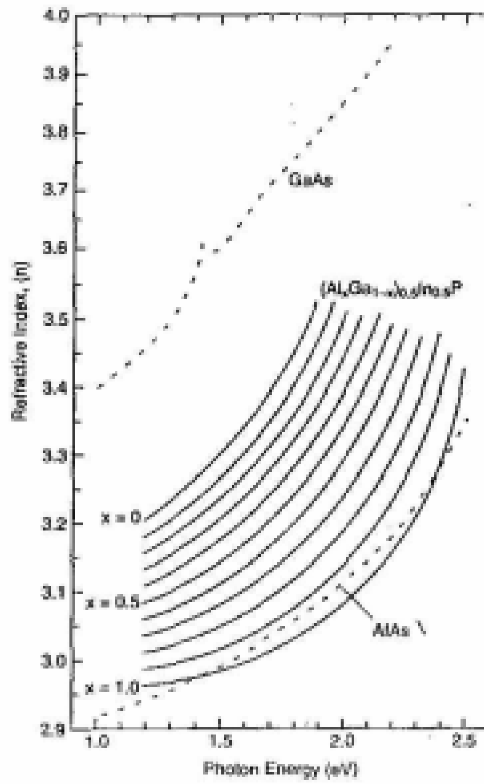

Fig. 1.3 Refractive index of AlGaInP from 3.0 (AlInP) to 3.2 (GaInP).

1.2 Introduction to AlGaInN Based Diodes

The GaN based LED was first manufactured by Nichia in 1997 [10-11]. From then on, it attracts much interest in this kind of material. Similar to the AlGaInP based semiconductor material, the AlGaInN alloy is made up of AlN, GaN and InN. The emitting wavelength is tunable from red to green spectral region [12-13]. Unfortunately, there are lots of difficulties in growing AlGaInN semiconductor material. The most difficult problem is that we cannot choose a substrate to fit the lattice constant of GaN based epitaxial layer. It is well known that lattice mismatch brings a diode with defects. The sapphire (Al_2O_3) substrate is widely used in growing this kind of material. The difference of lattice constant between sapphire and GaN is about 16.1 % [14]. Undoubtedly, we can expect that there are lots of defects in the diode. The density of defect in GaN diode could be more than ten thousand times higher than the AlGaInP one. Due to the fact that the structure of sapphire is much different from a usual semiconductor material, it cannot form cleaving faces in fabricating laser diode. On the other hand, this kind of substrate is insulator. Therefore, we cannot plate an electrode on it. As shown in Fig. 1.4, we coat electrode in one side when growing the GaN epitaxial layer on sapphire substrate. That is, we plate positive and negative electrodes on the same side. Alternatively, the GaN semiconductor material can be grown on SiC substrate too. The difference of lattice constant between SiC and GaN is about 3.5 % [14]. Furthermore, the structure of SiC is the same as a usual semiconductor material and it is a semiconductor. Nevertheless, the bandgap of SiC is

about 2.95 eV, which may cause light absorption when the emitting wavelength is shorter than 420 nm. Furthermore, the SiC substrate is expensive. Consequently, the SiC substrate is less utilized. Table 1.1 shows the comparison between sapphire and SiC substrates. It is difficult to grow a GaN based semiconductor material because the GaN epitaxial layers need to be grown under higher temperature (about 1050 ^{0}C). But the structure of the diode is stable after growing. It brings us long lifetime for use. As shown in Fig. 1.5, Nichia Inc. had ever grown high quality laser diode with ELOG substrate (by burying SiO_2 in buffer layer) [15]. The buried SiO_2 can block most defects, and the other defects are nearly centralized in one region and extend up side [16].

Table 1.1 Comparison between Al_2O_3 and SiC substrates.

	Al_2O_3	6-H SiC
Conductivity	No	Yes
Lattice mismatch	16.1%	3.5%
Thermal conductivity	0.46W/cm-K	4.9W/cm-K
Thermal expansion	Smaller than GaN, and GaN will create compressive strain	Smaller than GaN, and GaN will create tensile strain
Crystal size	2 inch diameter	1.5 inch diameter
Coast	Several Japanese dollar	10~15 Japanese dollar
Fabrication company	Union Carbite, Cyocera	Cree Research

At room temperature, the band gaps of AlN, GaN, and InN are 6.2 eV, 3.4 eV, and 1.9 eV, respectively, when the AlGaInN semiconductor material is grown on sapphire. The emitting wavelength of this kind of

material is tunable from red to green spectral region. Therefore, in growing AlGaInN diode emitting at longer wavelength, it is necessary to use higher mole composition of indium. However, the indium vaporizes easily when growing a diode. Therefore, it is hard in growing $In_xGa_{1-x}N$ when x is larger than 0.3. Presently, the semiconductor diode emitting at longer wavelength is mainly grown by AlGaInP based material.

In 1998, AlGaN cladding with modulation doping had been successfully grown. In general, electrons transport by thermal radiation and tunnel effect in super lattice structure. In the border between the double hetero structures, it contains kinks in band structure. These kinks will cause electric resistance in electrons transporting. With modulation doping, the band structures can be smoother and the electric resistance of the diodes can be lower.

Alike AlGaInP based semiconductor materials, the refractive index change of AlGaInN is small too. Consequently, we need to grow large numbers of DBR pairs for higher reflectivity. However, the defects of this kind of materials are huge in growing films. It is a challenge in growing AlGaInN based VCSEL. However, optically pumped ultra-violet VCSEL had grown by Redwing *et al.* [17].

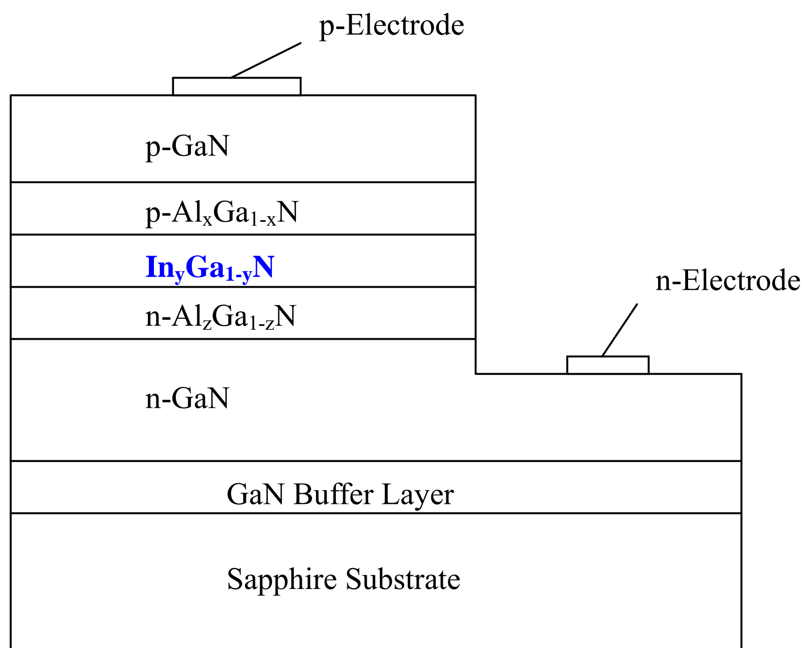

Fig. 1.4 Structure of AlGaInN based LED and LD.

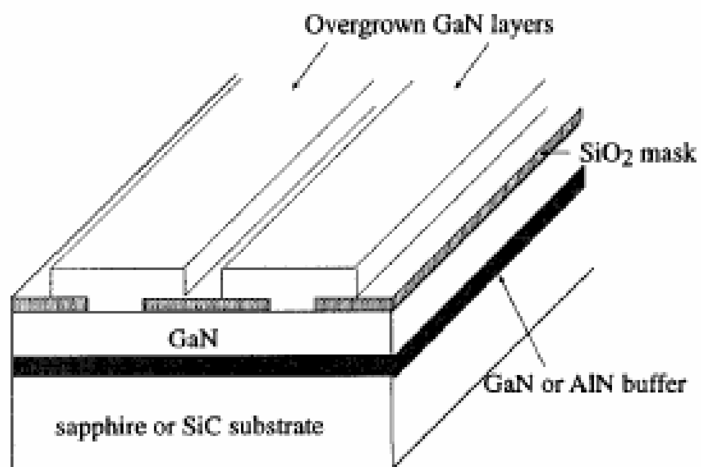

Fig. 1.5 High quality laser diode with ELOG substrate grown by Nichia Inc.

1.3 Introduction to VCSEL

The edge-emitting laser forms a cavity by cleaving and coating on it and the laser diode emits light perpendicularly to the grow axis. The current distribution in the active region is flat. By the theorem of diffraction, the distribution of laser spot in space is an ellipse [18]. It influences the size of the laser spot when the laser output is focused with a lens. The advantage of smaller laser spot is that we can increase the data density of an optical disk. Although we can decrease the ellipticity of the ellipse with gain guiding structure, we cannot get laser spot with perfect circle eventually.

As for VCSEL, as indicated by its name, it forms cavity vertically on diode [19]. In the early days, people used metal to form reflecting mirrors. However, because metal absorbs electromagnetic waves, the metal mirrors may absorb the light produced by the VCSEL. Afterwards, people take the idea of film interference into consideration. They grow DBR on n-type and p-type cladding by generating different materials of semiconductor and successfully grow a high performance VCSEL in the end [20].

One of the major advantages of VCSEL is that it emits a circular laser spot. It results in a smaller size when focused by a lens. Therefore, it is widely used in optical fiber communications [21-23].

A so-called DBR is constructed with films of different refractive indexes. The effective thickness must be a quarter of the emitting wavelength in each film. The use of DBR can also improve the light output efficiency of a light emitting diode (LED) [24-26]. As shown in Fig. 1.6,

the refractive index n_1 is lower than n_2, therefore the phase of light denoted (1) differs from the phase of light denoted (2) by π. If we want that the light denoted (3) to have constructive interference to light (2), the round trip difference between (2) and (3) must be odd integer times of a quarter of the wavelength. The effective thickness of medium (2) is therefore odd integer times of a quarter of the wavelength. Oppositely, the phase does not change when reflected by medium (1). We can prove that the effective thickness of medium (1) must be odd integer times of a quarter of the wavelength similarly.

We can get higher reflective efficiency with larger numbers of DBR. Nevertheless, with the increasing of DBR pairs we get larger electric resistance. In order to reduce the electric resistance and save the cost of the materials, we should use higher refractive index change of material to grow DBR. Furthermore, we can obtain smaller electric resistance with fewer DBR pairs. There are some other ways to reduce the electric resistance of the DBR. For example, we may grow grading structure on cladding or dope the cladding with the technique of modulation doping.

The cavity of a VCSEL is composed of active region and spacers. The spacers are located between the active region and the n-type or p-type DBR. Standing waves are formed within the cavity of the VCSEL. Generally, the effective cavity length is integer multiple of the emitting wavelength. Investigation shows that the VCSEL usually has the best performance when the cavity has a length of one wavelength. For longer cavity lengths, the stimulated emission rate in the active region is decreased, which leads to higher threshold current and lower output power.

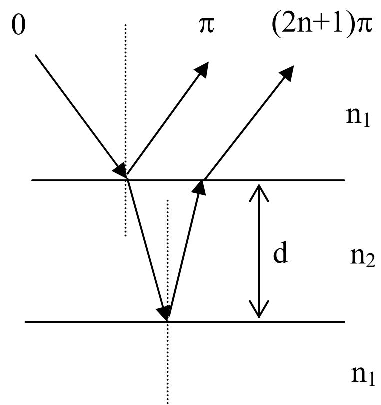

Fig. 1.6 Paths of light crossing the DBR.

References

[1] R. S. Kern, “Progress and status of visible light emitting diode technology,“ in Light-Emitting Diodes: Reach, Manufacturing, and Applications III, E. Fred Schubert, Ian T. Ferguson, H. Walter Yao, Editors, Proceeding of SPIE vol. 3621, pp. 16-27, 1999.

[2] G. B. Stringfellow and M. Georage Craford, High Brightness Light Emitting Diodes - Semiconductors and Semimetals Volume 48, Academic Press, San Diego, California, USA, 1997.

[3] T. Fukunaga, M. Wada, and T. Hayakawa, "High-power 0.8 μm InGaAsP/InGaP/AlGaAs single quantum well lasers with tensile-strained InGaP barrier," Jpn. J. Appl. Phys., vol. 38, pp. L387-L389, 1999.

[4] S. Kamiyama, T. Uenoyama, M. Mannoh, and K. Ohnaka, "Strain effect on 630 nm GaInP/AlGaInP multi-quantum well lasers," Jpn. J. Appl. Phys., vol. 33, pp. 2571-2578, 1994.

[5] I. Nomura, K. Kishino, A. Kikuchi, and Y. Kaneko, "600-nm-range GaInP/AlInP strained quantum well lasers grown by gas source molecular beam epitaxy," Jpn. J. Appl. Phys., vol. 33, pp. 804-810, 1994.

[6] H. Sugawara and M. Ishikawa, "Compensated-strain multiquantum-well active layer for InGaAlP-based visible light emitting diodes," Jpn. J. Appl. Phys., vol. 34, pp. L1458-L1460, 1995.

[7]P. S. Zory, Jr., Quantum Well Lasers, Academic Press, San Diego, California, USA, 1993.

[8] S. J. Chang, C. S. Chang, Y. K. Su, Senior Member, IEEE, P. T. Chang, Y. R. Wu, K. H. Huang, and T. P. Chen, "AlGaInP yellow-green light-emitting diodes with a tensile strain barrier cladding layer," IEEE Photon. Technol. Lett., vol. 9, pp. 1199-1201, 1997.

[9] S. J. Chang and C. S. Chang, "642-nm AlGaInP laser diodes with a triple tensile strain barrier cladding layer," IEEE Photon. Technol. Lett., vol. 10, pp. 651-653, 1998.

[10] S. Nakamura, M. Senoh, S. Nahama, N. Iwasa, T. Matushita, T. Mukai,

"InGaN/GaN/AlGaN-Based LEDs and Laser Diodes," MRS Internet Journal Nitride Semiconductor Research, vol. 3, Article 31, 1999.

[11] S. Nakamura and G. Fasol, The Blue Laser Diode, Springer-Verlag, Heidelberg, 1997.

[12] J. I. Pankove and T. D. Moustakas, Gallium Nitride (GaN) I – Semiconductors and Semimetals Volume 50, Academic Press, San Diego, California, USA, 1998.

[13] J. I. Pankove and T. D. Moustakas, Gallium Nitride (GaN) II – Semiconductors and Semimetals Volume 57, Academic Press, San Diego, California, USA, 1999.

[14] Industrial Material (in Chinese), vol. 6, pp. 140, 1998.

[15] S. Nakamura, Proc. IEEE Lasers and Electro-Optics Society 1997 Annual Meeting, 1997.

[16] S. C. Jain, M. Willander, J. Narayan and R. Van Overstraeten, "III – nitrides Growth, characterization, and properties," J. Appl. Phys., vol. 87, pp. 965-1006, 2000.

[17] J. M. Redwing, D. A. S. Loeber, N. G. Anderson, M. A. Tischler, and J. S. Flynn, "An optically pumped GaN-AlGaN vertical cavity surface emitting laser," Appl. Phys. Lett., vol. 69, pp. 1-3, 1996.

[18] Y. K. Kuo, Lecture Note of Semiconductor Lasers, 1999.

[19] H. Soda, Jpn. J. Appl. Phys., vol. 18, 2329, 1979.

[20] F. A. Kish, F. M. Steranka, D. C. DeFevere, D. A. Vanderwater, K. G. Park, C. P. Kuo, T. D. Osentowski, M. J. Peanasky, J. G. Yu, R. M. Fletcher, D. A. Steigerwald, and M. G. Craford, "Very high-efficiency semiconductor wafer-bonded transparent-substrate $(AI_xGa_{1-x})_{0.5}In_{0.5}P/GaP$ light-emitting diodes," Appl. Phys. Lett., vol. 64, pp. 2839-2841, 1994.

[21] D. M. Kuchta and C. J. Mahon, "Mode selective loss penalties in VCSEL optical fiber transmission links," IEEE Photon. Technol. Lett., vol. 6, pp. 288-290, 1994.

[22] H. Kosaka, M. Kajita, M. Yamada, and Y. Sugimoto, "A 16x16 optical full-cross-bar connection module with VCSEL-array push/pull module and polymer-waveguide coupler connector," IEEE Photon. Technol. Lett., vol. 9, pp. 244-246, 1997.

[23] M. Bruensteiner, G. C. Papen, J. Poulton, S. Tell, R. Palmer, K. Giboney, D. Dolfi,

and S. Corzine, "3, 3-V CMOS pre-equalization VCSEL transmitter for gigabit multimode fiber links," IEEE Photon. Technol. Lett., vol. 11, pp. 1301-1303, 1999.

[24] H. Sugawara, K. Itaya, H. Nozaki, and G. Hatakoshi, "High-brightness InGaAlP green light-emitting diodes," Appl. Phys. Lett., vol. 61, pp. 1775-1777, 1992.

[25] H. Sugawara, K. Itaya, and G. Hatakoshi, "Hybrid-type InGaAlP/GaAs distributed bragger reflectors for InGaAlP light-emitting diodes," Jpn. J. Appl. Phys., vol. 33, pp. 6195-6198, 1994.

[26] A. K. Dutta, K. Ueda, K. Hara, and K. Kobayashi, "High brightness and reliable AlGaInP-based light-emitting diode for POF data links," IEEE Photon. Technol. Lett., vol. 9, pp. 1567-1569, 1997.

Chapter 2. The Electrical and Optical Properties of AlGaInP Based Multi-Quantum Well Vertical-Cavity Surface-Emitting Lasers

High-performance AlGaInP vertical-cavity surface-emitting lasers (VCSEL) are useful in polymer-based optical fiber communication. Polymer optical fibers (POF) with polymethy1 methacrylate (PMMA-d8) cores have three transition windows near 670 nm, 780 nm, and 850 nm, respectively [1]. In this work, we study the 670-nm AlGaInP based multi-quantum well structure with AlGaInP and AlGaAs based distributed Bragg reflector (DBR), respectively, with the PICS3D (Photonic Integrated Circuit Simulator in 3D) simulation program purchased from Crosslight Software Inc. [2]. The laser performance of the AlGaInP VCSELs with these two different kinds of DBRs and the reflectivity spectra of the DBRs themselves are explored in detail in this work. In the mean time, the effect of temperature variance on the characteristics of the VCSELs and DBRs are also investigated. On the other hand, the properties between the electric input power and the laser output power are studied. Finally, the performance of the VCSEL with an optimized structure is explored.

2.1 Characteristics of AlGaInP Lasers and Polymer Optical Fibers

The AlGaInP based semiconductor laser material that is lattice matched to the GaAs substrate is capable of emitting in the red, orange, and yellow-green region [3-6]. Furthermore, the quaternary AlGaInP alloy compound, which has a direct transition in this wavelength region, is useful in these wavelength ranges. The AlGaInP laser diodes emitting at 650 nm have lots of important applications, such like laser pointers, digital versatile disk (DVD) pick-up head to increase higher storage in a compact disk, outdoor display, etc [7-9]. In addition, by introducing a strained layer into the active layer the property of a laser diode can be improved (i.e., shift the peak wavelength, increase the output power, and so on). This property allows us to design a useful laser diode in short wavelength with high output power [10].

High-performance AlGaInP laser diodes and LEDs are useful in polymer-based optical fiber communication [11-14]. Polymer optical fibers (POF) with polymethy1 methacrylate (PMMA-d8) cores have three transition windows, separately centered near 670 nm, 780 nm, and 850 nm, respectively. Figure 2.1 shows the transmission loss spectra of PMMA-d8 core POF. It is obvious that one transmission window is centered near 670 nm.

The VCSEL emitting at 670 nm had been widely studied in the past few years [15-20]. It is directly perceived through the sense that the AlGaInP based MQW with AlGaInP DBRs will contribute better performance on account of lattice matching and the innate qualities of the

same material. However, the AlGaAs DBR can also be used in this kind of diode. It is interesting to know that which one is better in terms of optical and electrical properties of the laser performance.

In general, a VCSEL emitting near 670 nm is useful in short-distance fiber communication due to its higher frequency in transportation and leak of far-distance transition [21]. Particularly, a short wavelength light, like 670 nm, can transfer data in higher than 1000 mega bits per second [22]. Hence, it is useful in high-speed optical fiber communication in the future.

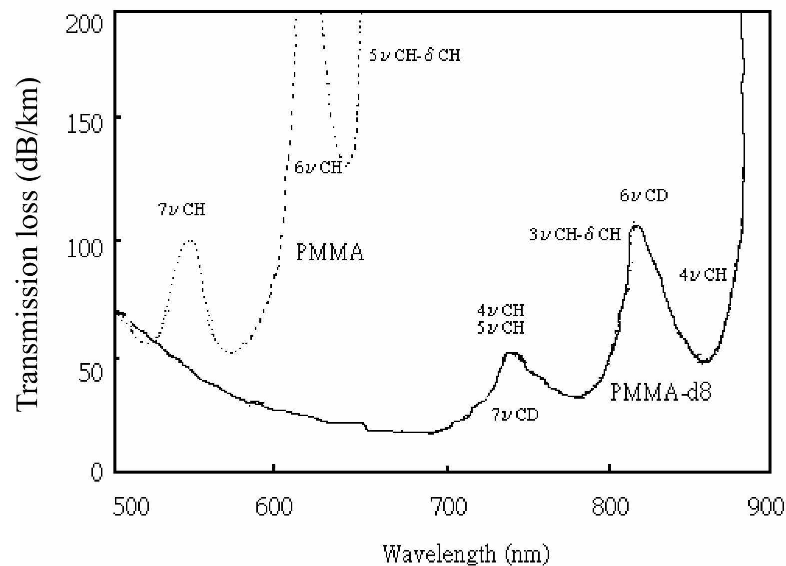

Fig. 2.1 Transmission loss spectra of PMMA-d8 core POF.

2.2 Structures of the Laser Diodes Under Study

Theoretically, by changing the composition of the multi-quantum wells (MQWs), we can get different peak wavelength of the AlGaInP based semiconductor lasers. In PICS3D simulation, the following formula is used to express the energy bandgap of the $(Al_xGa_{1-x})_{0.5}In_{0.5}P$ semiconductor material, $E_g(x)$, at 300 K [23]:

$$E_g(x)=1.891+0.49x+0.0025x^2, \text{ (eV)} \quad (1)$$

where the variable x is the composition of aluminum. The formula of the effective masses of the electrons and holes in the AlGaInP based material is defined as following in our simulation:

$$m_e=(0.0124+0.0915x)m_0, \quad (2)$$

$$m_h=0.56m_0, \quad (3)$$

where m_e is the effective mass of the electrons in AlGaInP, m_h is the effective mass of the holes in AlGaInP, and m_0 is the free-electron mass.

Besides, the following formula is used to represent the refractive index of the $(Al_xGa_{1-x})_{0.5}In_{0.5}P$ semiconductor material [24], n:

$$n^2-1=\frac{E_d}{E_o}+\frac{E_dE_p^2}{E_o^3}+\frac{E_dE_p^4}{2E_o^3(E_o^2-E_\Gamma^2)}\ln\left(\frac{2E_o^2-E_\Gamma^2-E_p^2}{E_\Gamma^2-E_p^2}\right). \quad (4)$$

The E_p equals to the energy of the injecting light and E_d, E_o, and E_Γ are defined as following:

$$E_d=35.79-1.16x, \quad (5)$$

$$E_o=4.17+0.49x, \quad (6)$$

$$E_\Gamma=1.89+0.67x, \quad (7)$$

where the variable x equals to the composition of aluminum.

Firstly, we know that one of the POF with PMMA-d8 cores has a transmission window near 670nm. In this study, we designed a 670-nm VCSEL with compressively strained well by numerical simulation. Secondly, we compare the performance of the distributed Bragger reflectors made of AlGaInP and AlGaAs in 670-nm AlGaInP MQW VCSELs.

Figures 2.2 (a) and 2.2 (b) show the structure of the AlGaInP based MQW VCSELs designed to be studied in this PICS3D numerical simulation. The radiuses of the two devices are both defined as 10 μm, and they have the same composition except DBRs.

The AlGaInP epitaxial layers were grown on 30-pairs n-doped AlInP/GaInP n-DBRs, which have thickness of 52.3 nm and 47.7 nm for each layer respectively for the 1/4 lambda of 670nm DBR design. The doping level of the 30-pairs n-type high-reflecting DBRs is equal to 2.0×10^{24} m^{-3}. The refractive indices of AlInP and GaInP are 3.149 and 3.512, respectively.

Following the n-DBR, the rest of the VCSEL consists of a 89.79 nm n-$(Al_{0.5}Ga_{0.5})_{0.5}In_{0.5}P$ n-Spacer ($n=1.0\times10^{24}$ m^{-3}), an undoped active region, a 89.79 nm p-$(Al_{0.5}Ga_{0.5})_{0.5}In_{0.5}P$ p-spacer ($p=1.0\times10^{24}$ m^{-3}), and 20-pairs p-doped AlInP/GaInP p-DBRs. The refractive index is 3.29663 of each spacer layer. The spacer is defined as 2-lambda optical cavity length of 670nm design for the total thickness of MQWs larger than 1 lambda. The

doping level of the 20-pairs p-type output coupling DBRs is equal to 3.0×10^{24} m^{-3}.

Similarly, the reflective indices of AlAs and $Al_{0.5}Ga_{0.5}As$ are 2.92 and 3.285, and the corresponding thicknesses are 57.4 nm and 51 nm. The active region of these two diodes consists of five pairs of 20nm/20nm $Ga_{0.44}In_{0.56}P/(Al_{0.5}Ga_{0.5})_{0.5}In_{0.5}P$ compressively strained MQWs. The average reflective index is 3.4 and the total thickness is 220 nm.

Both of them have 20 pairs of p-type DBRs and 30 pairs of n-type DBRs, and we can expect that the laser light will emit from the p-type DBRs. For convenience, we denote the device with AlGaInP DBRs as device 1, and the other as device 2. These two structures were simulated in the same simulation condition.

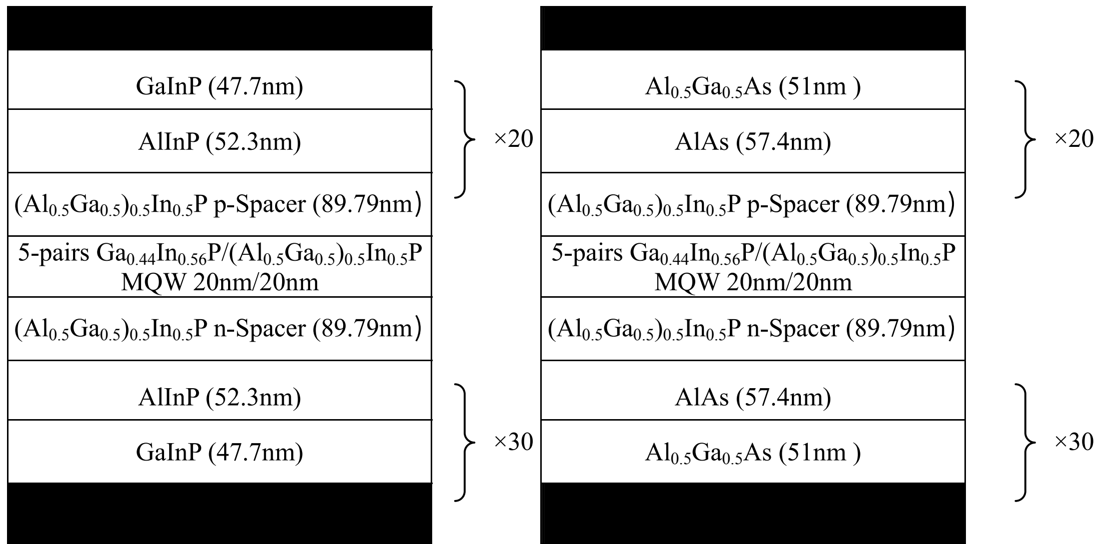

Fig. 2.2 Structures of the two VCSEL devices with different DBR under study: (a) AlGaInP, (b) AlGaAs.

2.3 The Electrical and Optical Properties of the VCSELs

Figures 2.3 (a) and 2.3 (b) show the reflectivity spectra for different pairs of DBRs with AlInP/GaInP and AlAs/$Al_{0.5}Ga_{0.5}As$ films, respectively. These figures indicate the reflectivity spectrum of the DBR as a function of the DBRs pair number. With the increasing of the DBR pair number, the reflectivity of DBR becomes higher, and the bandwidth becomes narrower.

The AlAs/$Al_{0.5}Ga_{0.5}As$ DBRs have higher reflectivity than AlInP/GaInP DBRs under equal pairs. This is in our anticipation because the index difference between AlAs and $Al_{0.5}Ga_{0.5}As$ (0.365) is a little higher than that between AlInP and GaInP (0.363). It may influence the characteristics of the VCSELs in latter discussion, since the DBRs play an important role in VCSEL. When the pair number is 10, the reflectivity in Figs. 2.3 (a) and 2.3 (b) is 91% and 93.5%, respectively. Furthermore, when the pair number is 20, the reflectivity in Fig. 2.3 (a) and 2.3 (b) is 98.675% and 98.704%.

We choose 20 and 30 pairs as output-coupling and high-reflecting DBRs, for that more pair numbers is not necessary and it will increase the resistance when we add voltage to operate. Moreover, it is worth to note that the bandwidth of AlAs/$Al_{0.5}Ga_{0.5}As$ DBRs is wider than that of AlInP/GaInP DBRs. It is convenient for real device design, because if the laser wavelength is a little shifted, the DBRs can still be utilized. By the way, we take these two kinds of materials as DBRs to grow VCSEL in 10 μm diameter to show which one is better.

Figures 2.4 (a) and 2.4 (b) show the log of electron concentration when

the injection current is 11.19 mA. The electron distribution in the active region in device 1 and device 2 are equal. However, in the n-DBR and p-DBR region, the electron concentration of device 2 is higher than that of device 1. That is due to the fact that the average energy band gap of AlAs and $Al_{0.5}Ga_{0.5}As$ (about 1.95 eV) is smaller than the average energy band gap of GaInP (about 2.254 eV).

The concentration in five quantum wells is not equivalent. The reason is that the potential near the p-type spacer is lower than that near the n-type spacer for electrons. We know that the electron tends to stay in low electric potential. So, the concentration in the well near p-type spacer is higher than that near n-type spacer.

Figures 2.5 (a) and 2.5 (b) are the log of hole concentration when the injection current is 11.19 mA. The hole concentration in p-DBR of device 2 is a little higher than that of device 1. This is due to the same reason of the electron distribution difference in Figs. 2.4 (a) and 2.4 (b).

However, the concentration in the well near p-type spacer is higher than that in the well near n-type spacer. The hole mobility is much larger than the electron one, and the drift velocity of holes is slower than that of electron; therefore, there are more holes confined in the well near p-type spacer. Holes have attractive force to electrons; this may be another reason why there are more electrons in the well near p-type spacer.

The inhomogeneous distribution of electrons and holes may cause the unequal stimulated recombination rate in the five wells. The more electrons and holes concentration is, the higher stimulated recombination rate is. Figure 2.6 shows the stimulated recombination rate in the active region.

Obviously, the rate in the well nearest the p-type spacer is higher than that in the well nearest the n-type spacer.

Figure 2.7 shows the relation between the injection current and the laser output power. The threshold current of device 1 and device 2 are 13.86 mA and 10.47 mA, respectively. The slope efficiency of device 1 is 0.87 W/A, and that of device 2 is 0.95 W/A. This shows that the laser efficiency of device 2 is better than that of device 1. That is because the reflectivity of AlGaAs based DBRs is superior to that of AlGaInP based ones under equal pair numbers.

Figures 2.8 (a) and 2.8 (b) show the I-V curves of device 1 and device 2. Comparing these curves, we find that the two devices have the same critical voltage of 1.7 V. When the voltage is above the critical value, the curve of device 2 is sharper than that of device 1. This means that device 2 has smaller electrical resistance. This is good for laser operation because we can get higher current with the same voltage. When we inject equal current into device 1 and device 2, the consumed electric power of device 2 is smaller. Combining Fig. 2.7 and Fig. 2.8, we can get the relation between electric power and laser output power.

Figures 2.9 (a) and 2.9 (b) are the power transformation curves of device 1 and device 2. The laser output power of device 2 is larger under equal input electric power, and the slope efficiency of device 2 (0.39) is also higher than that of device 1 (0.3). There are two reasons for this result, one is that device 2 has higher laser output power than device 1 when the injection current is equal, and the other is that the resistance of device 2 is smaller. We can also get the threshold power of device 1 and device 2 by

mathematical extension method.

The threshold power of device 1 and device 2 are 30.5 mW and 21.56 mW, respectively. The higher power transition ratio means the lower thermal creation. The size of VCSEL is very small in comparison to the edge-emitting lasers, so the thermal effect is more serious than the edge-emitting diodes. We do not like to have much heat created in operation because it will reduce the laser efficiency. From Figs. 2.9 (a) and 2.9 (b), we conclude that device 2 has higher power transformation efficiency and less thermal generation in operation.

If we deduce the core radius of the device, the carrier density will enhance under the same injection current. This is helpful in reducing the threshold current. In Figs. 2.10 (a) and 2.10 (b), we compare the L-I curves of device 1 and device 2 with core radius of 10 μm and 5 μm. After we reduce the core radius to 5 μm, the threshold current becomes lower than the original devices. Furthermore, the threshold current of the device with 5 μm radius is one to four in comparison with the device with 10 μm one. That is due to that the carrier density is four times of that owes to the original one.

In Fig. 2.10 (a) the threshold current of the device with radius 5 μm is 3.5 mA, and that in Fig. 2.10 (b) is 2.7 mA. The slope efficiency of the smaller devices in Fig. 2.10 (a) and Fig. 2.10 (b) are both equal to that of the larger devices. This result is reasonable and easy to understand if we transfer the unit of slope efficiency from mW/mA to (mW-cm^{-3})/(mA-cm^{-3}).

Figures 2.11 (a) and 2.11 (b) show the I-V curves of device 1 and

device 2 of variant core radius. Both of Figs. 2.11 (a) and 2.11 (b) show that the resistance of device increases with decreasing core radius. However, the critical voltage does not change with the device size. That is because that the thickness of the undoped region, i.e., the active region, does not change.

From Figs. 2.11 (a) and 2.11 (b), we can find that under the equal voltage the current of the device with 5 μm radius is four times of that owes to the device with 10 μm radius when the voltage is higher than 1.7 V. That means the resistance is proportional to $1/\text{radius}^2$. We can get more detailed information after we go a step further to plot the power transformation curves.

Figures 2.12(a) and 2.12 (b) are the power transformation curves of the two devices with variant core radius. We may find that the threshold electric power is independent of the core radius of the device and the slope efficiency is proportional to the cross-section. It means that we can get higher power transformation effect by reducing the core of the device, and that will not decrease the slope efficiency of devices.

Let's now introduce gain-guiding structure into the device. Figures 2.13 (a) and 2.13 (b) are the structures of the devices. The radius of p-type DBR is 5 μm, while the spacer, the active region, and the n-type DBR have 10 μm radius. The doping concentration and the composition remain unchanged with that shown in Figs. 2.2 (a) and 2.2 (b). For convenience, we denote the device with AlGaInP DBRs as device 3, and the other as device 4. The upper electrode is a ring of 1 μm in width.

The L-I curves of the devices with gain-guiding structures are shown

in Figs. 2.14 (a) and 2.14 (b). The laser efficiency of the device with AlGaAs based DBRs is still better than that of the device with AlGaInP based DBRs; i.e., it still has lower threshold current and higher slope efficiency. The threshold current of the device with AlGaInP DBRs is 8.87 mA, and that of the other device is 6.4 mA. Although the device with gain-guiding structure has lower threshold current in comparison with the 10 μm radius device, however, the slope efficiency is worse. The slope efficiency is 0.74 mW/mA and 0.81 mW/mA of the two devices with gain-guiding structure, which are about 0.15 lower than the devices with 10 μm radius cores.

Figures 2.15 (a) and 2.15 (b) and Figs. 2.16 (a) and 2.16 (b) show the I-V curves and the power transformation curves of the two devices. The critical voltage remains equal to the device without gain-guiding structure, and the resistance is larger than that of the 10 μm core radius device but smaller than that of the 5 μm core radius one. The power transformation curves show that the output power of device 3 and device 4 are higher than the device 1 and device 2 under equal input electric power, but the slope efficiency of them is worse.

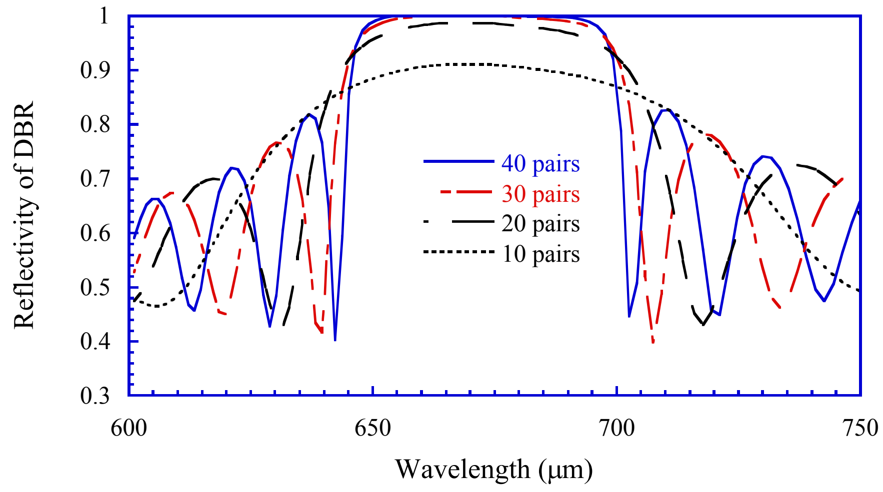

Fig. 2.3 (a) Reflectivity spectra for different pairs of DBR (AlGaInP).

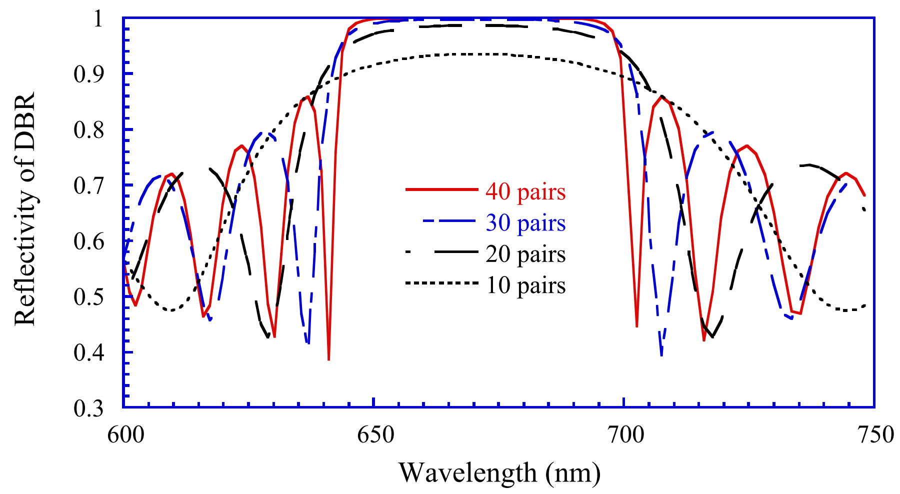

Fig. 2.3 (b) Reflectivity spectra for different pairs of DBRs (AlGaAs).

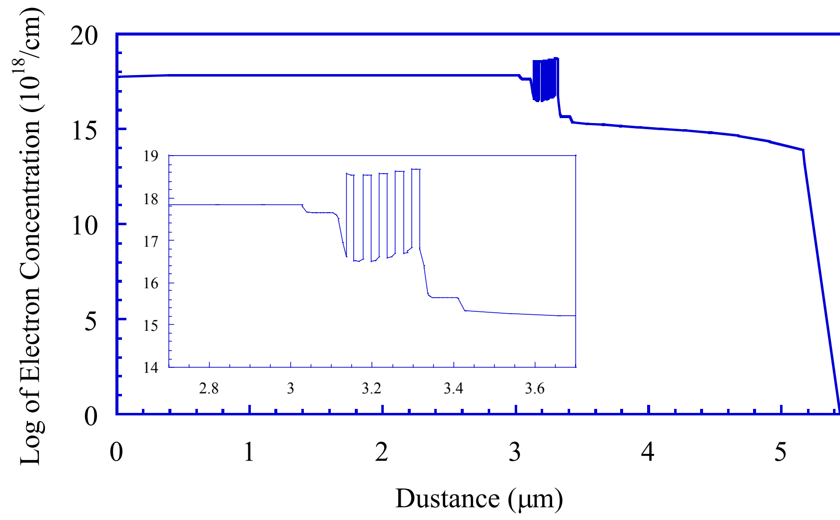

Fig. 2.4 (a) Log of electron concentration when the injection current is 11.19 mA (AlGaInP).

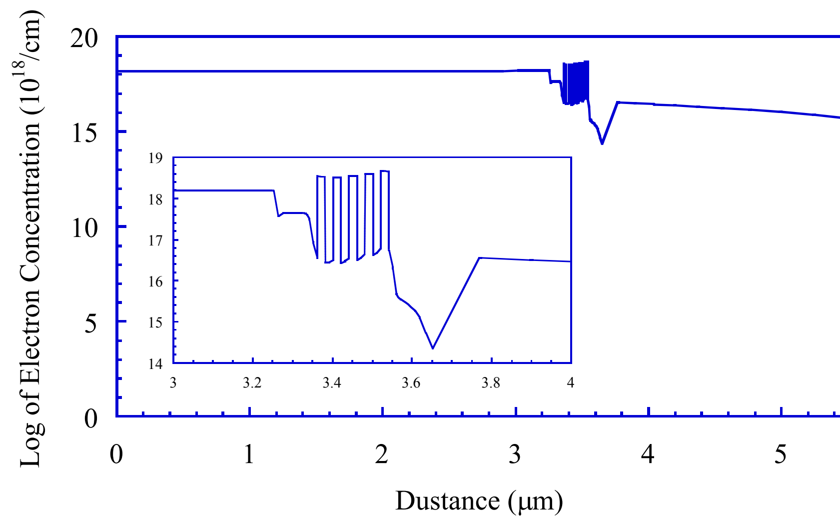

Fig. 2.4 (b) Log of electron concentration when the injection current is 11.19 mA (AlGaAs).

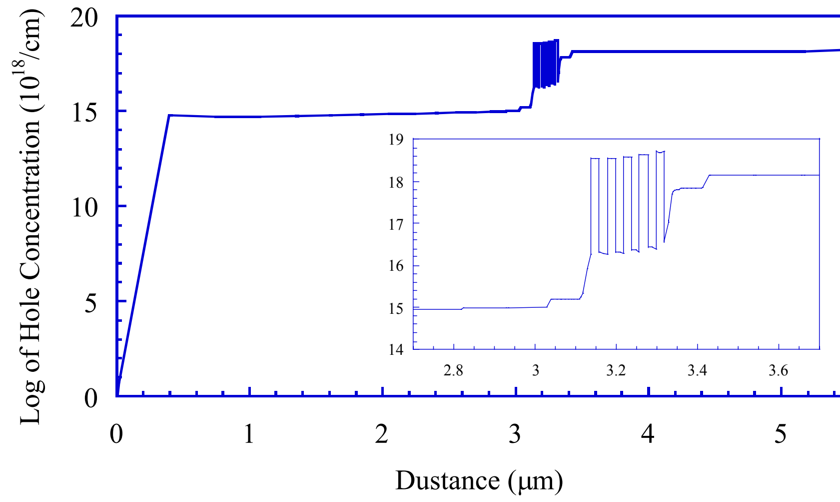

Fig. 2.5 (a) Log of hole concentration when the injection current is 11.19 mA (AlGaInP).

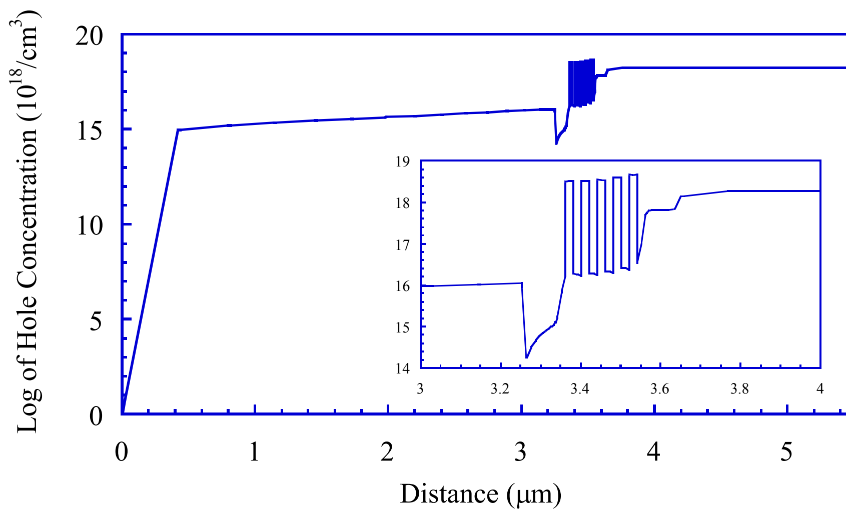

Fig. 2.5 (b) Log of hole concentration when the injection current is 11.19 mA (AlGaAs).

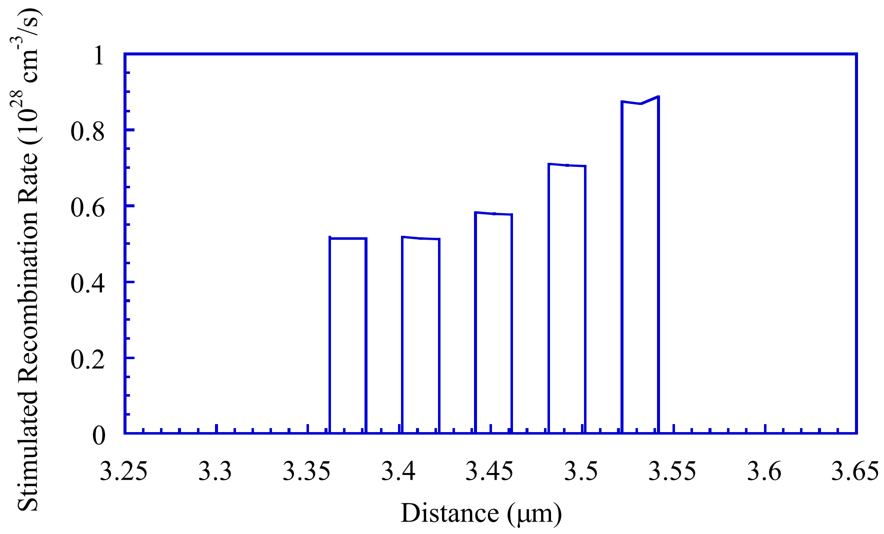

Fig. 2.6 Stimulated recombination rate in the active region.

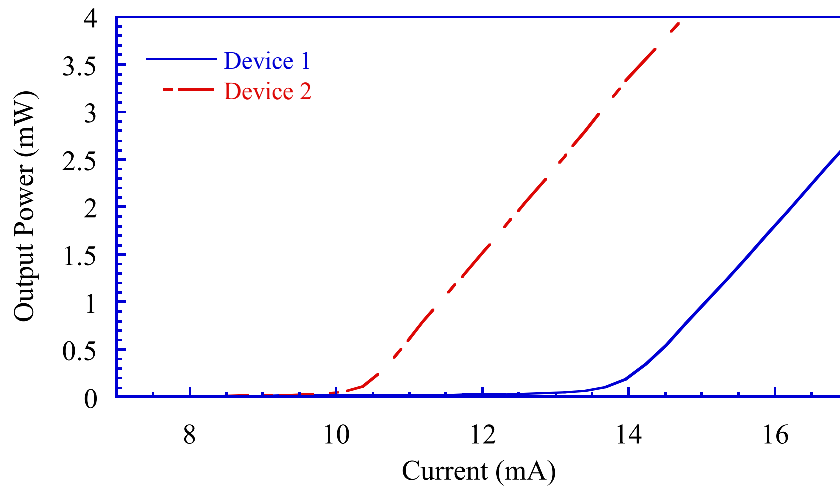

Fig. 2.7 L-I curves of these two diodes.

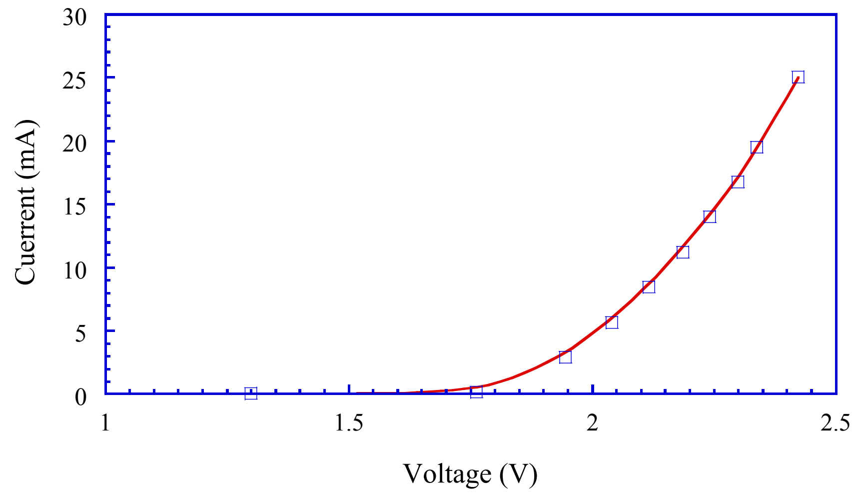

Fig. 2.8 (a) I-V curves of the diode (AlGaInP).

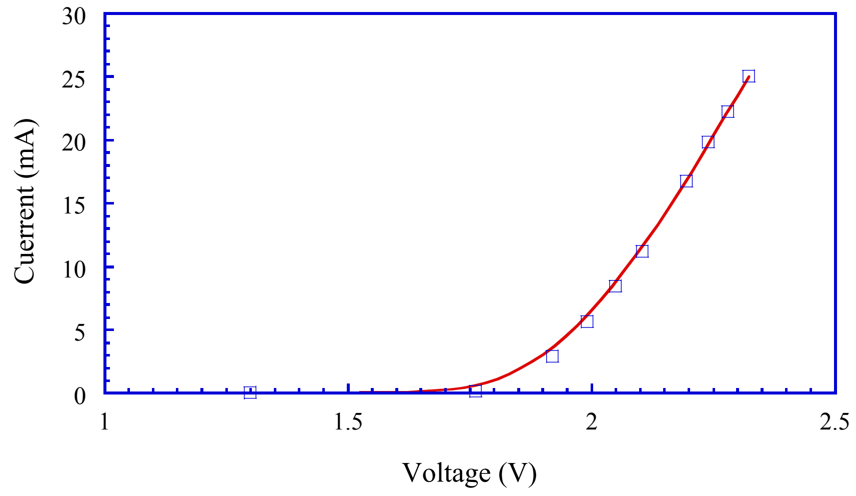

Fig. 2.8 (b) I-V curves of the diode (AlGaAs).

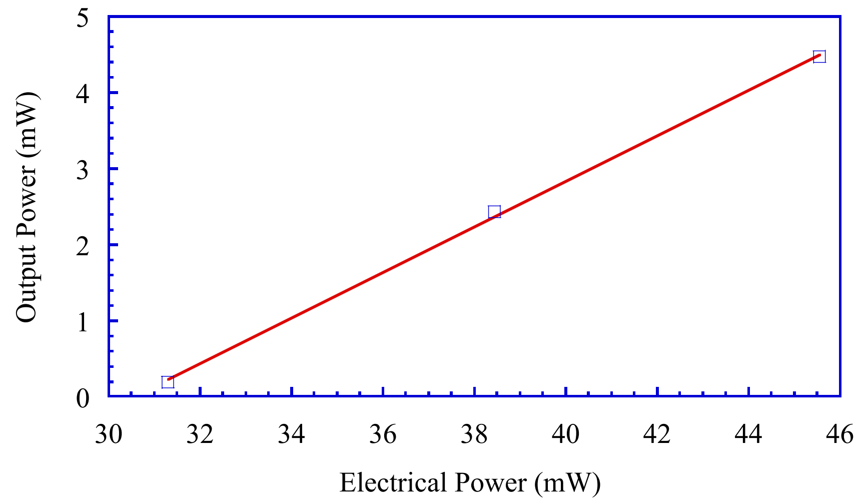

Fig. 2.9 (a) Power transformation curves of the diode (AlGaInP).

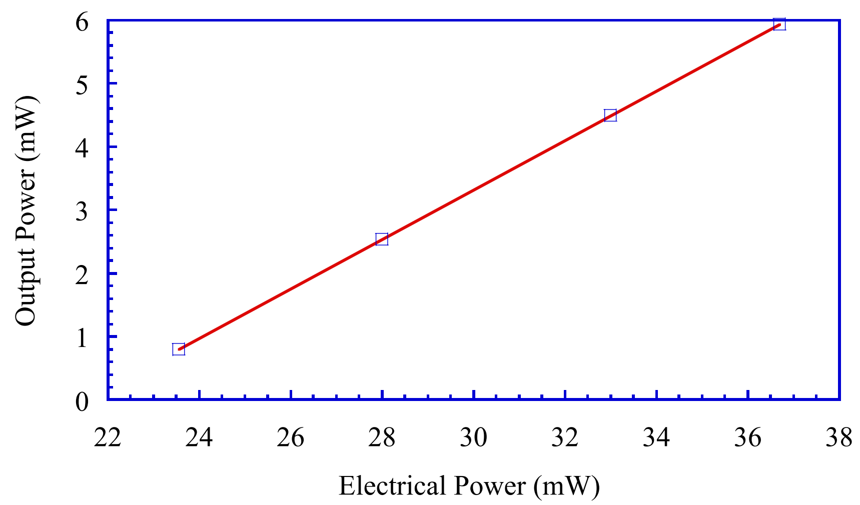

Fig. 2.9 (b) Power transformation curves of the diode (AlGaAs).

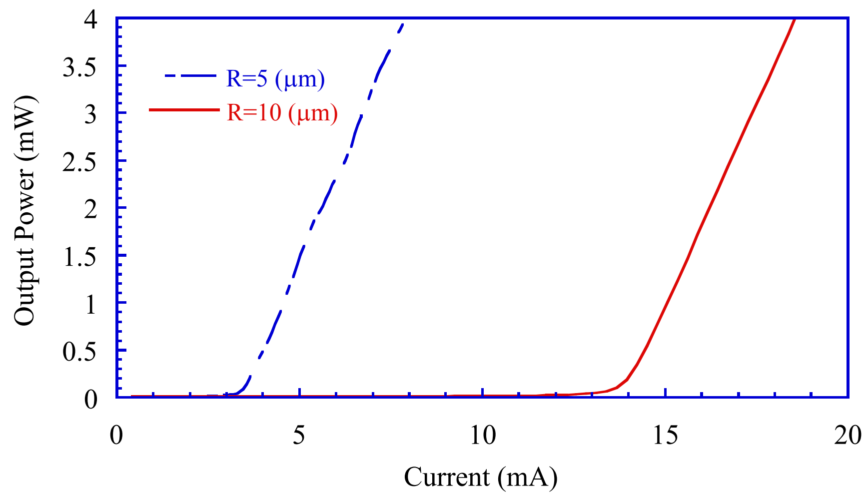

Fig. 2.10 (a) L-I curves of the diode with core radius of 10 μm and 5 μm (AlGaInP).

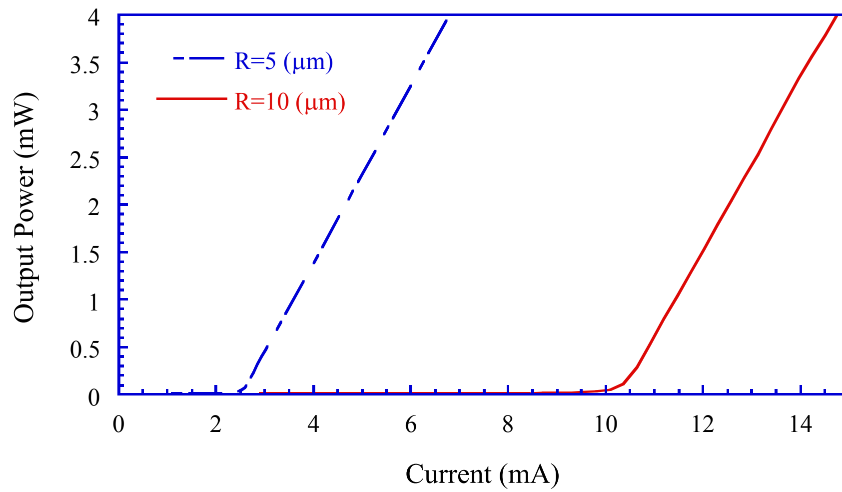

Fig. 2.10 (b) L-I curves of the diode with core radius of 10 μm and 5 μm (AlGaAs).

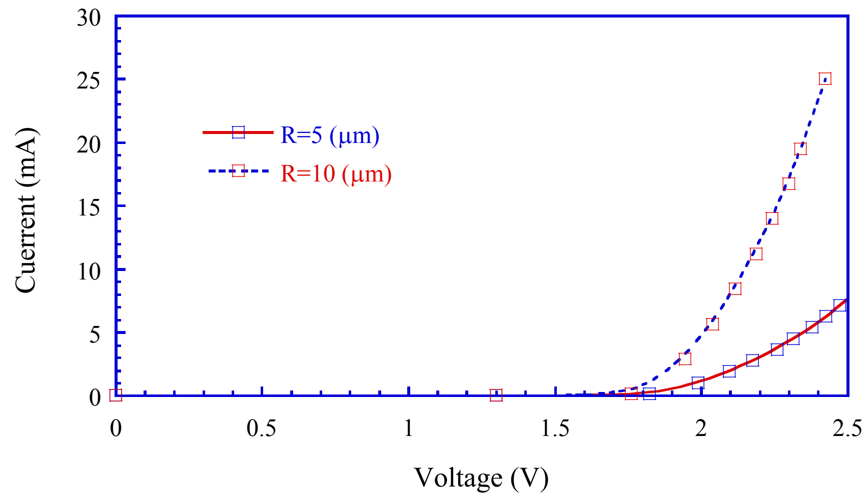

Fig. 2.11 (a) I-V curves of the diode of variant core radius (AlGaInP).

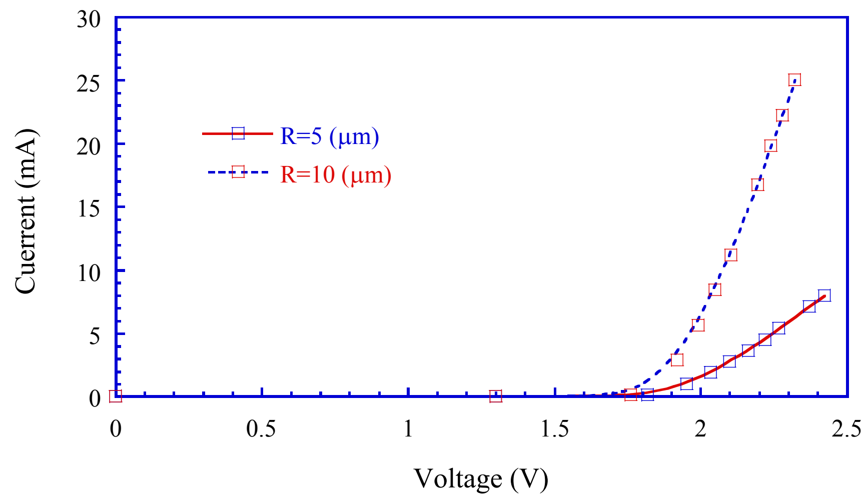

Fig. 2.11 (b) I-V curves of the diode of variant core radius (AlGaAs).

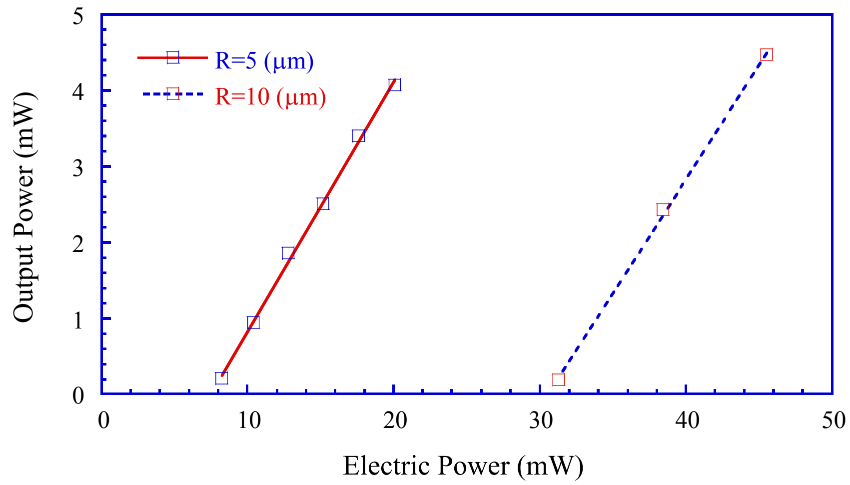

Fig. 2.12 (a) Power transformation curves of the diode with variant core radius (AlGaInP).

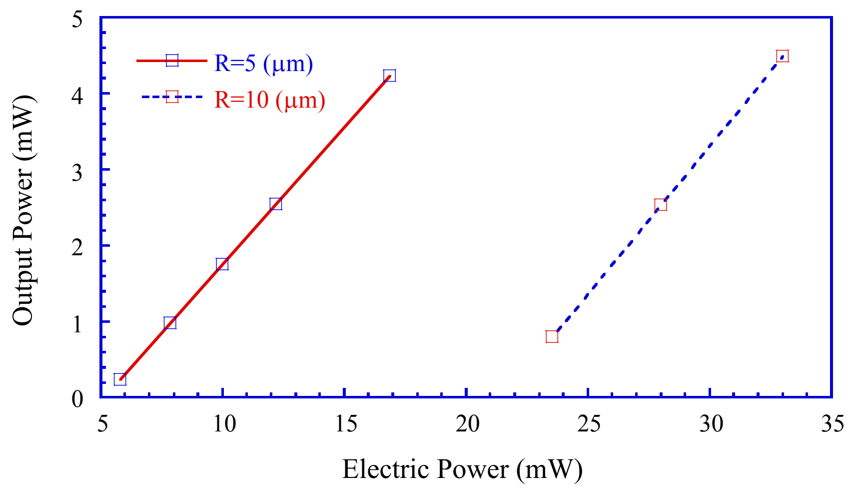

Fig. 2.12 (b) Power transformation curves of the diode with variant core radius (AlGaAs).

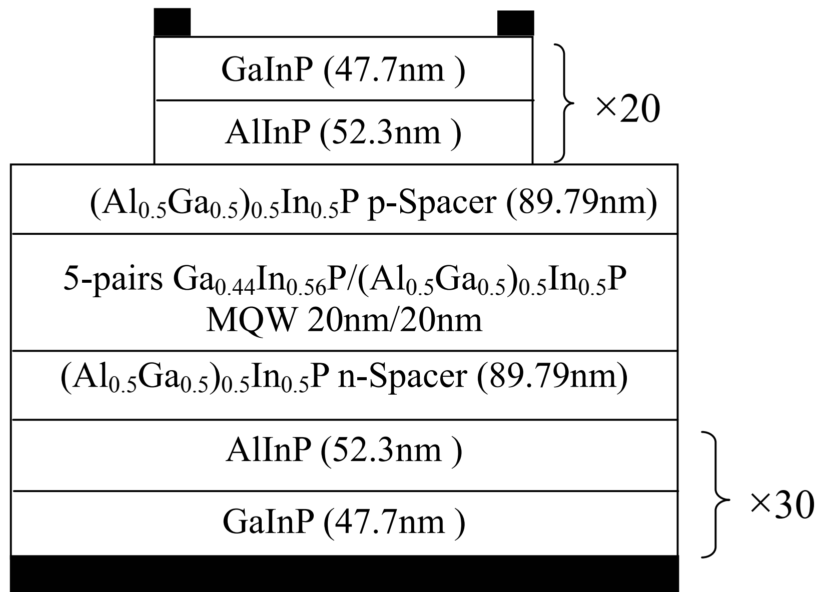

Fig. 2.13 (a) Structure of the VCSEL devices with current-spreading (AlGaInP).

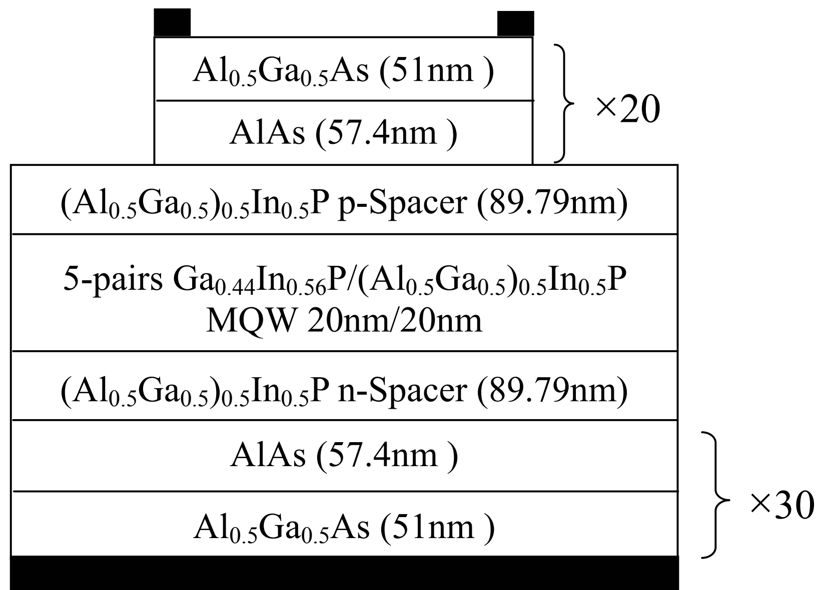

Fig. 2.13 (b) Structure of the VCSEL devices with current-spreading (AlGaAs).

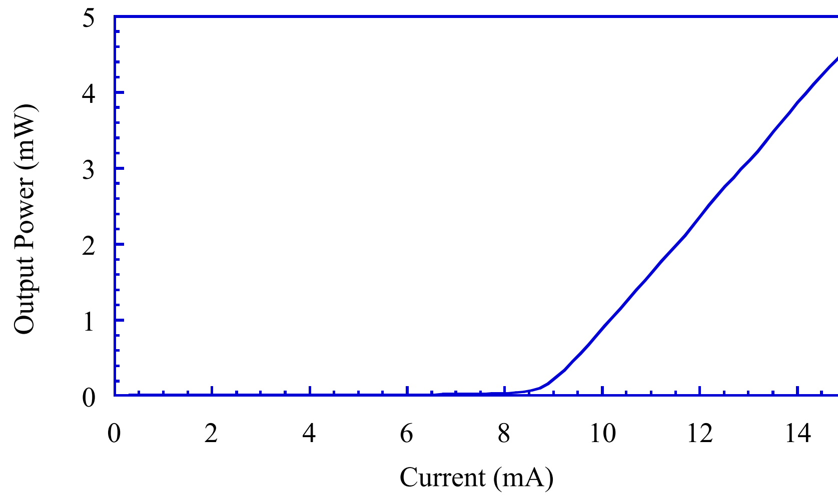

Fig. 2.14 (a) L-I curves of the devices with gain-guiding structures (AlGaInP).

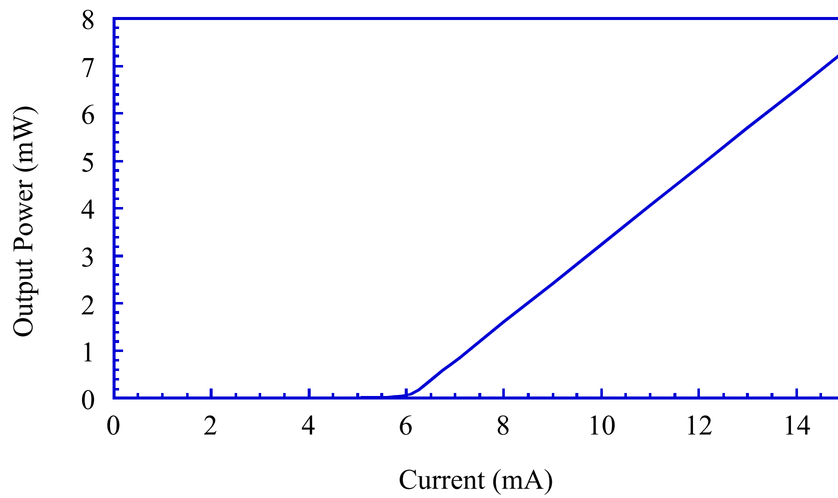

Fig. 2.14 (b) L-I curves of the devices with gain-guiding structures (AlGaAs).

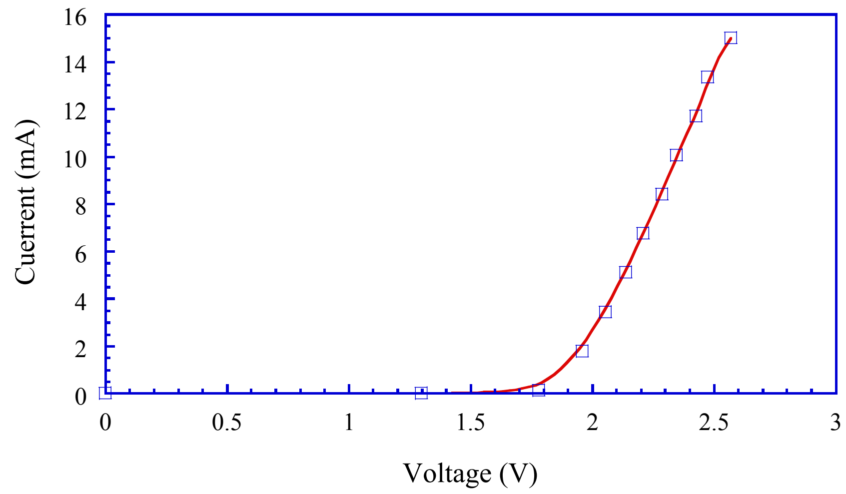

Fig. 2.15 (a) I-V curves of the devices with gain-guiding structures (AlGaInP).

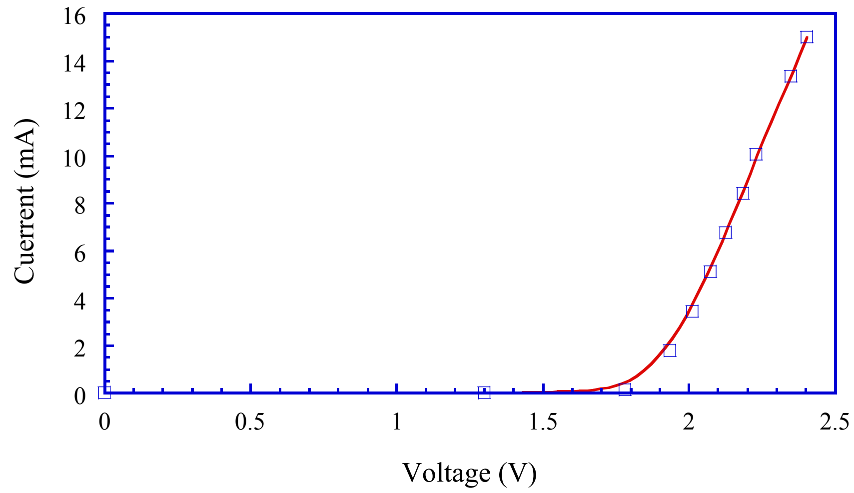

Fig. 2.15 (b) I-V curves of the devices with gain-guiding structures (AlGaAs).

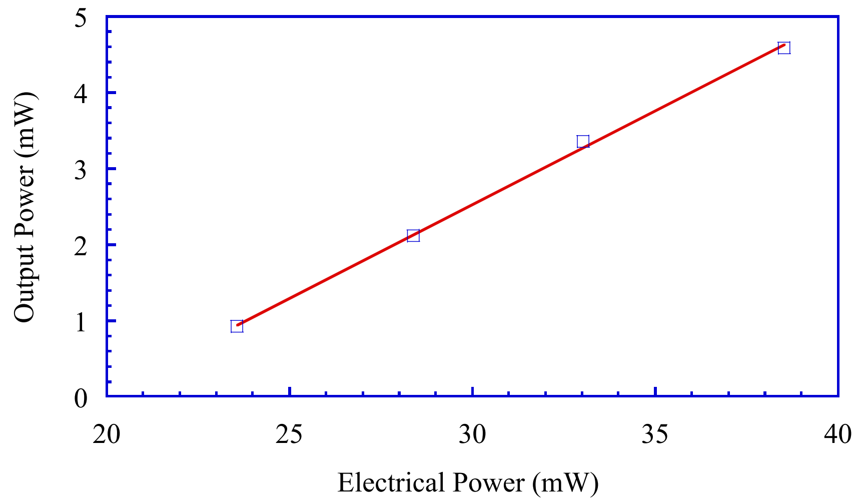

Fig. 2.16 (a) Power transformation curves of the diode with gain-guiding structures (AlGaInP).

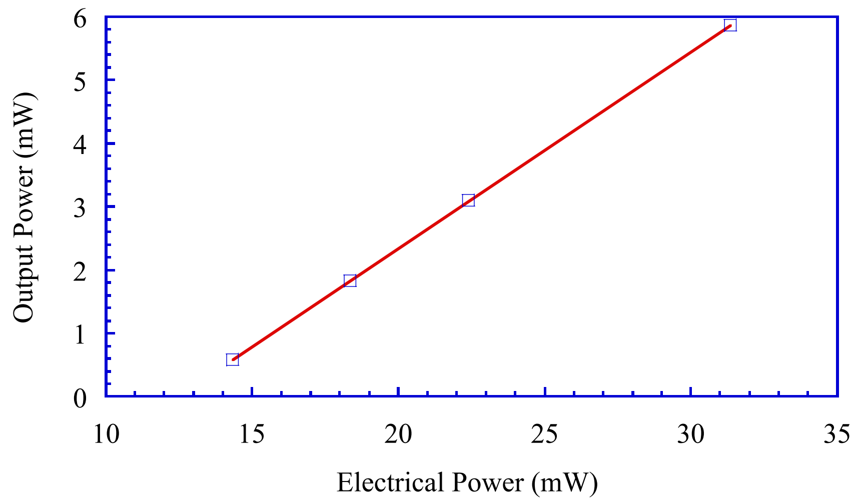

Fig. 2.16 (b) Power transformation curves of the diode with gain-guiding structures (AlGaAs).

2.4 Discussion

The performance of the quantum well near the p-type region is superior to that near the n-type region for higher electron and hole concentration for 670-nm AlGaInP VCSEL, and that makes the unequal stimulated recombination rate in the five quantum wells. The electron and hole concentrations in AlGaAs DBRs region are higher than that in AlGaInP DBRs region under the same current.

The reflection coefficient of DBRs enhances with increasing pairs of DBRs, and the bandwidth of reflective spectra decreases when the DBR pairs increase. The reflection coefficient of the AlGaAs DBRs is higher than that of the AlGaInP DBRs under equal pair numbers of DBRs and the bandwidth of the AlGaAs DBRs is wider, too. By the way, if we design a 670-nm AlGaInP multi-quantum well VCSEL with AlGaAs based and AlGaInP based DBRs, the performance of laser with AlGaAs based DBRs is better than that with AlGaInP based DBRs. The threshold current of laser with AlGaAs based DBRs is lower, the slope efficiency is higher, and the resistance is smaller. Therefore, we may get higher laser output power with equal injection current and smaller voltage, i.e., smaller input electric power. This implies that induced thermal energy of the laser with AlGaAs based DBRs is lower when operating, and that is good for the small volume VCSEL.

The VCSEL with smaller core radius has higher current density when we inject equal current; therefore, the threshold current is lower. However, the slope efficiency will not change with core radius because if we want to

get equal power density we must inject current density. The disadvantage is that the resistance of VCSEL with smaller core radius is larger, but it does not influence the slope efficiency. So we have lower threshold power and higher power transition effect with smaller core radius.

The current spreading structure is another way to lower the threshold current, and its resistance is between the smaller and larger diodes. However, the transformation efficiency from electric power to laser output power of this structure will decrease. The improvement on laser performance with this structure is not as good as that we reduce the core radius directly, although it is better than the original device.

References

[1] T. Kaino, K. Jinguji, and S. Nara, "Low loss poly (methylmethacrylate-d8) core optical fibers," Appl. Phys. Lett., vol. 42, pp. 567-569, 1983.

[2] PICS3D Manual Ver. 3.1 (Crosslight Software Inc., 1997)

[3] R. S. Kern, “Progress and status of visible light emitting diode technology, “ in Light-Emitting Diodes: Reach, Manufacturing, and Applications III, E. Fred Schubert, Ian T. Ferguson, H. Walter Yao, Editors, Proceeding of SPIE, vol. 3621, pp. 16-27, 1999.

[4] G. B. Stringfellow and M. Georage Craford, High Brightness Light Emitting Diodes - Semiconductors and Semimetals Volume 48, Academic Press, San Diego, California, USA, 1997.

[5] H. C. Casey, Jr. and M. B. Panish, Heterostructure Lasers, New York, Academic, 1978, pt. B, p. 3.

[6] H. Sugawara, K. Itaya, H. Nozaki, and G. Hatakoshi, “High-brightness InGaAlP green light-emitting diodes,“ Appl. Phys. Lett., vol. 61, pp. 1775-1777, 1992.

[7] O. Imafuji, T. Fukuhisa, M. Yuri, M. Mannoh, A. Yoshikawa, and K. Itoh, “Low operating current and high-temperature operating of 650-nm AlGaInP high-power laser diodes with real refractive index guided self-aligned structure,“ IEEE J. Sel. Top. Quantum Electron., vol. 5, pp. 721-728, 1999.

[8] S. J. Chang, C. S. Chang, Y. K. Su, P. T. Chen, Y. R. Wu, K. H. Huang, and T. P. Chen, "Chirped GaAs-AlAs distributed Bragg reflectors for high brightness yellow-green light-emitting diodes," IEEE Photon. Technol. Lett., vol. 9, pp. 182-184, 1997.

[9] S. J. Chang, C. S. Chang, Y. K. Su, P. T. Chen, Y. R. Wu, K. H. Huang, and T. P. Chen, "AlGaInP yellow-green light-emitting diodes with a tensile strain barrier cladding layer," IEEE Photon. Technol. Lett., vol. 9, pp. 1199-1201, 1997.

[10] Peter S. Zory, Jr., Quantum Well Lasers, Academic Press, Inc. San Diego, New York, USA, 1993.

[11] A. Kumar, A. Suzuki, K. Kurihara, F. Miyasaka, H. Hotta, and K. Sugita, "High-brightness, AlGaInP-based, visible light-emitting diode for efficient coupling with POF," IEEE Photon. Technol. Lett., vol. 7, pp. 1134-1136, 1995.

[12] M. Hayashi, M. Tsuji, K. Makita, K. Nyu, S. Yamazaki, K. Sujita, and K. Taguchi, "GaAs pin-photodiodes with an AlGaInP window layer for use in 650-nm wavelength GI-POF data links," IEEE Photon. Technol. Lett., vol. 8, pp. 833-835, 1996.

[13] S. J. Chang and C. S. Chang, "650 nm AlGaInP/GaInP compressively strained multi-quantum well light emitting diodes," Jpn. J. Appl. Phys. vol. 37, pp. L653-L655, 1998.

[14] B. V. Dutt, J. H. Racette, S. J. Anderson, F. W. Scholl, and J. R. Shealy, "AlGaInP/GaAs red edge-emitting diodes for polymer optical fiber application," Appl. Phys. Lett., vol. 53, pp. 2091-2092, 1988.

[15] J. A. Lott, R. P. Schneider JR., K. D. Choquette, S. P. Kilcoyne and J. J. Figiel, "Room temperature continuous wave operation of red vertical cavity surface emitting laser diode," Electron. Lett., vol. 29, pp. 1693-1694, 1993.

[16] R. P. Schneider, Jr., K. D. Choquette, J. A. Lott, K. L. LEAR, Member, IEEE, J. J. Figiel, and K. J. Malloy, Member, IEEE, "Efficient room-temperature continuous-wave AlGaInP/AlGaAs visible (670 nm) vertical-cavity surface emitting laser diodes," IEEE Photon. Technol. Lett., vol. 6, pp. 313-316, 1994.

[17] M. H. Crawford, R. P. Schneider, Jr., K. D. Choquette, and K. L. Lear, Member, IEEE, "Temperature-dependent characteristics and single mode performance of AlGaInP-based 670-690-nm vertical-cavity surface-emitting lasers," IEEE Photon. Technol. Lett., vol. 7, pp. 724-726, 1995.

[18] R. P. Schneider, Jr., M. H. Crawford, K. D. Choquette, K. L. Lear, S. P. Kilcoyne, J. and J. Figiel, "Improved AlGaInP-based red (670-690 nm) surface-emitting lasers with novel C-doped short-cavity epitaxial design," Appl. Phys. Lett., vol. 67, pp. 329-331, 1995.

[19] D. M. Kuchta, Member, IEEE, R. P. Schneider, K. D. Choquette, and S. Kilcoyne, "Large- and small-single modulation properties of red (670 nm) VCSEL's," IEEE Photon. Technol. Lett., vol. 8, pp. 307-309, 1996.

[20] S. J. Sweeney, G. Knowles, and T. E. Sale, "Evaluating the continuous-wave performance of AlGaInP-based red (667 nm) vertical-cavity surface-emitting laser using low-temperature and high-pressure techniques," Appl. Phys. Lett., vol. 78, pp. 865-867, 1995.

[21] A. K. Dutta, K. Hara, K. Kobayashi, and N. Nagashima, "Impedance, modulation

response and equivalent-circuit of 650 nm surface emitting type light-emitting diode for POF data-links," Solid-State Electron., vol. 42, pp. 1787-1791, 1998.

[22] G. Hatakoshi, K. Takaoka, and M. Ishikawa, "InGaAlP red VCSELs," Proc. IEEE Lasers and Electro-Optics Society 2000 Annual Meeting, vol. 2, pp. 722-723, 2000.

[23] A. A. Mbaye, and C. Verie, "Electronic structure of trimetallic III-V alloys: The Al1-x-zGaxInzP system, " Phys. Rev. B, vol. 29, pp. 2756-2758, 1984.

[24] Y. Kaneko and K. Kishino, “Refractive indices measurement of (GaInP)m/(AlInP)n quasi-quaternaries and GaInP/AlInP multiple quantum wells,” J. Appl. Phys., vol. 76, pp. 1809-1818, 1994.

Chapter 3. Numerical Study on an Electrically Pumped 440-nm InGaN Vertical-Cavity Surface-Emitting Laser

There is a growing interest in short wavelength III-nitride optoelectronic devices for high density optical storage, optical fiber communication, high-brightness white light emitting diodes (LED), flame detection, and fluorescence based chemical sensing application. The InGaN multi-quantum well edge emitting laser diodes and light emitting diodes had been successfully demonstrated in the past few years [1-4].

However, there are relatively few reports on short wavelength InGaN vertical cavity surface emitting laser (VCSEL). One of the major difficulties in growing III-nitride distributed Bragger reflectors (DBR) is wafer cracking due to lattice mismatch between the AlGaN and GaN. It is important for a VCSEL with DBR to have flat surfaces [5-7]. Quite recently, with the use of low-temperature AlGaN inter layers the Sandia National Laboratory, USA, was able to grow 60-pair GaN/AlGaN DBR with high crystal quality [8]. By using low-temperature AlGaN interlayer, it will reduce the stress and form better surface in each layer of DBR.

In this work, we investigate the reflectivity spectra of the GaN/AlGaN DBR numerically with an advanced simulation program PICS3D [9-10]. Optical and electrical performance, including the light output characteristics and the characteristic temperature, of a blue InGaN VCSEL that uses the GaN/AlGaN DBR is studied. Finally, we tried to optimize the structure by changing the number of quantum wells and DBR pairs. Hopefully this kind of VCSEL will be practicable in the future.

The optical properties of an electrically pumped blue InGaN vertical-cavity surface-emitting laser are numerically investigated. The distributed Bragg reflector consists of $GaN/Al_{0.27}Ga_{0.73}N$ that has a reflectivity of 99.3% for the high reflecting mirror (50 pairs) and 96.4% for the output-coupling mirror (30 pairs) at 440 nm. The threshold current of this vertical-cavity surface-emitting laser, which has three $In_{0.14}Ga_{0.86}N/In_{0.01}Ga_{0.99}N$ quantum wells in the active region, is about 38 mA at room temperature. We take this structure as a standpoint and design a VCSEL with a threshold current lower than 10 mA at the same current density.

3.1 Characteristics of InGaN MQW Lasers

The AlN/GaN distributed Bragger reflector (DBR) and optically pumped III-nitride VCSELs have been studied previously by Redwing *et al.* [1-4]. However, the electrically pumped III-nitride VCSELs have not been demonstrated to our knowledge.

Figure 3.1 is the relation between indium composition and the peak wavelength of bulk InGaN. The peak wavelength has red shift with increasing indium composition. From the figure, we find that the peak wavelength increases almost linearly with indium composition and if we want to get 440 nm emitting wavelength, the indium composition in the bulk must be about 0.132. However, if we want to design a quantum well to emit at 440 nm, the indium composition must increase because the quantum well has a shorter peak wavelength than bulk under equal indium composition. According to Ref. 11, we choose the indium composition as 0.14.

In PICS3D simulation, the following formula is used to express the energy bandgap of the bulk InGaN and InGaN/InGaN semiconductor material, $E_g(x)$, at 300 K [12,13]:

$$E_g(x)=1.95x + 3.4(1-x) - bx(1-x) \text{ (eV)}, \quad (1)$$

where the variable x is the composition of indium and b is the bowing parameter. The formula of effective masses of the electrons and the holes in the InGaN material is defined as following in our simulation:

$$m_e=0.22m_0 - 0.11x\, m_0, \quad (2)$$

$$m_h=0.8m_0, \quad (3)$$

where m_e is the effective mass of the electrons in InGaN, m_h is the effective mass of the holes in InGaN, and m_0 is the free-electron mass.

Figure 3.2 is the peak wavelength of the quantum well as a function of well width when the composition of indium in well and barrier are 0.14 and 0.01. From the figure we see that the quantum effect starts to reveal when the well width is about 6 nm, and the blue shift of the wavelength is more obvious with the decreasing well width. When the well width is 4 nm, the peak wavelength is 439 nm. Therefore, for our purpose to design a 440 nm VCSEL and for the convenience of laser cavity design, we choose the well width to be 4 nm.

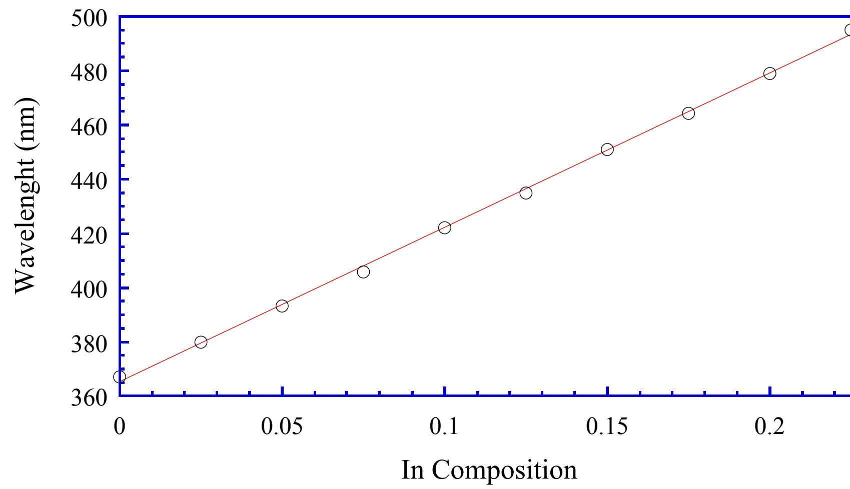

Fig. 3.1 Relation between indium composition and peak wavelength of bulk InGaN.

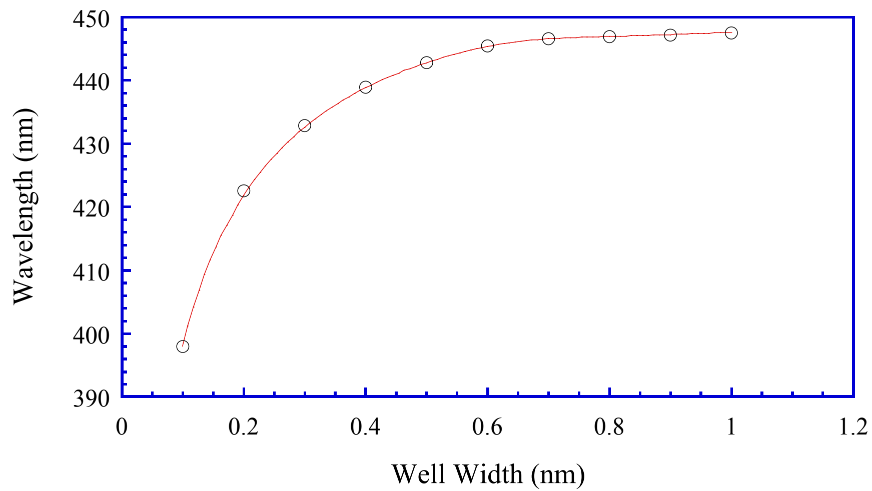

Fig. 3.2 Wavelength as a function of well width when the composition of indium in well and barrier are 0.14 and 0.01.

3.2 Structures of the Diodes

In year 2000, N. Nakada *et al.* published in Applied Physics Letter about growing InGaN light emitting diode with $Al_{0.27}Ga_{0.73}N$ DBR on it. They showed that the LED with fifteen pairs of $Al_{0.27}Ga_{0.73}N$ DBR has a better light output performance than a LED without DBR. The reflectivity spectra measured by ultraviolet-visible spectrometer of 15 pairs of $GaN/Al_{0.27}Ga_{0.73}N$ DBR fabricated by N. Nakada *et al.* are shown in Fig. 3.3.

For comparison, we simulated the fifteen pairs of $Al_{0.27}Ga_{0.73}N$ DBR by PICS3D simulation program. Figure 3.4 shows the reflectivity spectra of 15 pairs of $GaN/Al_{0.27}Ga_{0.73}N$ DBR simulated by PICS3D simulation program. As expected, the simulation result of $Al_{0.27}Ga_{0.73}N$ DBR will have a better performance than that of experimental result. The spectrum obtained by the simulation program is similar to the result reported in the paper when the indices of the high-index layers and low-index layers in DBR are defined as 2.5067 and 2.3906, respectively.

The VCSEL has lots of applications such like high density DVD pick-up head, light source of optical fiber communications and so on [14]. In the past few years, the VCSEL with other kinds of semiconductor materials had been successfully fabricated and studied. It is a pity that the electrically pumped VCSELs with III-nitride material have not been grown and well studied yet [15-16]. It is interesting to investigate the performance of the electrically pumped VCSEL with $GaN/Al_{0.27}Ga_{0.73}N$ DBR emitting at 440 nm. In the thesis, we study the 440-nm VCSEL with $GaN/Al_{0.27}Ga_{0.73}N$

DBR with a simulation program. Hopefully this work may be helpful for the development of the advanced 440-nm VCSEL in the future.

Figure 3.5 shows the cross-sectional structure of the blue InGaN VCSEL under study. There are three quantum wells in the active region. The $In_{0.14}Ga_{0.86}N$ well has a thickness of 4 nm and the $In_{0.01}Ga_{0.99}N$ barrier has a thickness of 5 nm. The materials used for the DBR are GaN for the high-index layers and $Al_{0.27}Ga_{0.73}N$ for the low-index layers, similar to those used by Nakada *et al.* in their blue LED structure, which have thickness of 43.9 nm and 46.0 nm for each layer respectively. The doping levels of the 30-pair p-type output coupling DBR and the 50-pair n-type high-reflecting DBR are both equal to 1.0×10^{18} cm^{-3}. The aperture diameter is 10 μm for the output coupling DBR and 20 μm for the high-reflecting DBR. The thickness of both the n-spacer and the p-spacer is 70 nm.

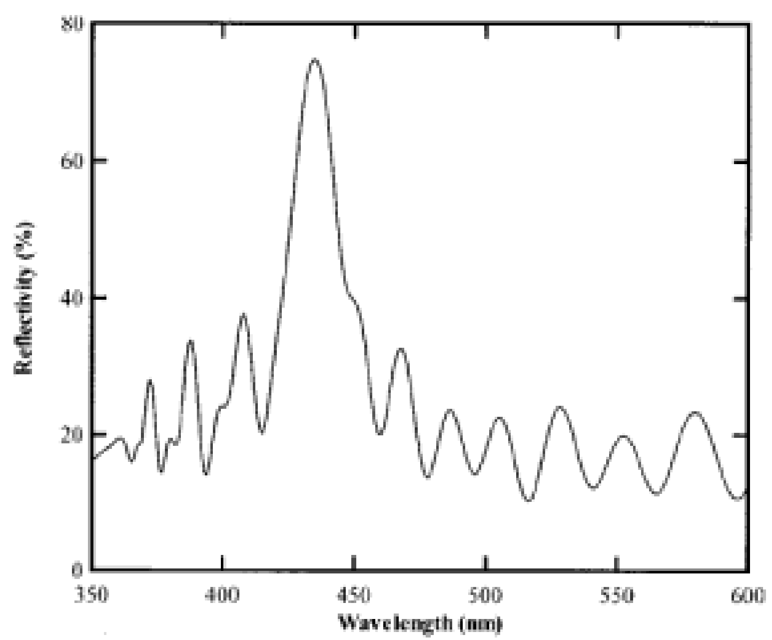

Fig. 3.3 Reflectivity Spectra of 15 pairs of GaN/$Al_{0.27}Ga_{0.73}N$ DBR.

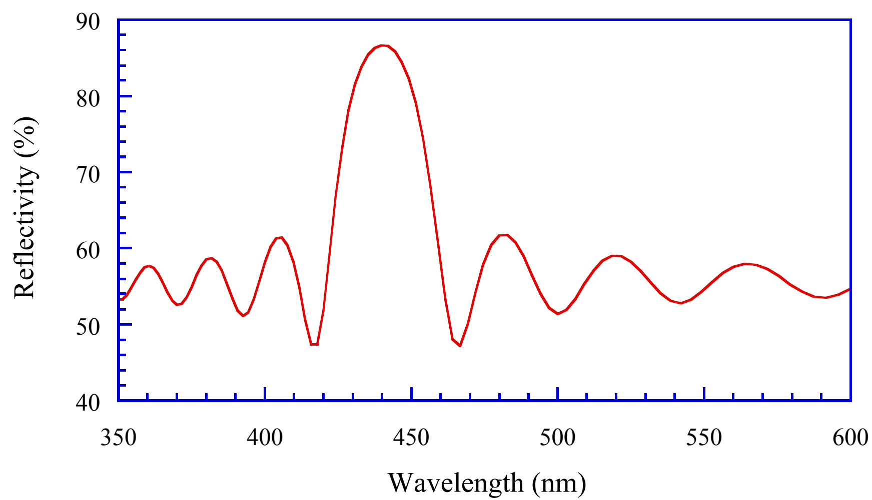

Fig. 3.4 Reflectivity Spectra of 15 pairs of GaN/$Al_{0.27}Ga_{0.73}N$ DBR simulated by PICS3D simulation program.

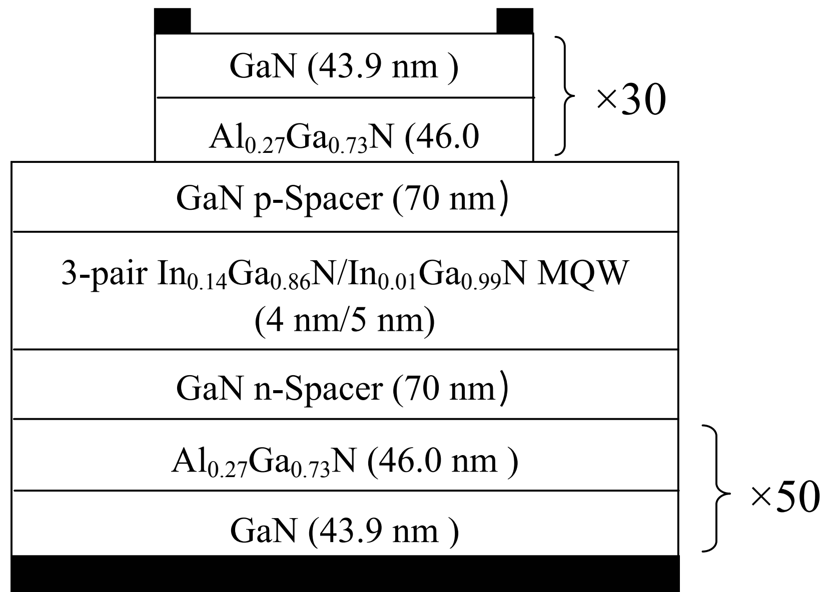

Fig. 3.5 Cross-sectional structure of the blue InGaN VCSEL under study.

3.3 The Electrical and Optical Properties of the VCSELs

Figure 3.6 shows the reflectivity spectra of the GaN/$Al_{0.27}Ga_{0.73}N$ DBR when the pair number of the DBR is equal to 10, 20, 30, 40, 50 and 60. It is obvious that the maximum reflectivity of the DBR increases and the high-reflecting bandwidth (full width at half maximum) decreases when the pair number increases. The GaN/$Al_{0.27}Ga_{0.73}N$ DBR has a maximum reflectivity of 0.795 at the designed laser wavelength, 440 nm, and a bandwidth of about 43 nm when the pair number is 10. The maximum reflectivity equals to 0.914, 0.964, 0.984, 0.993, and 0.996 and the bandwidth equals to 32 nm, 22 nm, 20 nm, 18 nm, and 17 nm when the pair number is 20, 30, 40, 50, and 60 respectively.

For the simulation of the optical performance of the InGaN VCSEL, the internal loss that includes the losses due to the absorption and the nonradiative recombination is assumed to be 5000 m^{-1}, which is higher than those for other III-V laser diodes but is reasonable for the III-nitride materials. Figure 3.7 shows the relation between the laser output power and the injection current, i.e., the L-I curve, of the InGaN VCSEL under study at room temperature, which has a threshold current of about 37.6 mA and a slope efficiency of about 0.84 mW/mA.

Figures 3.8 (a) and 3.8 (b) show the mode spectra when the injection current is at 33.9 mA (10% below the laser threshold) and 41.4 mA (10% above the laser threshold), respectively. From the simulation results we note that the laser wavelength is 439.2 nm and the mode spacing between the dominant mode and the first side mode is about 9.0 nm. The side mode

suppression ratio is equal to 17.4 dB when the injection current is equal to 33.9 mA. The side mode suppression ratio increases abruptly to a value of 35.4 dB when the injection current is increased to 41.4 mA. Figure 3.9 shows the side mode suppression ratio as a function of the injection current, which has an abrupt variation when the injection current is near the laser threshold. We may also find threshold current from this figure if we do differentiation of this curve and find the maximum. When the injection current is above the laser threshold, the side mode suppression ratio tends to saturate with increased injection current and has a value of about 37.6 dB when the injection current is at 44 mA.

The distribution of the electron and hole concentrations obtained at an injection current of 41.4 mA are shown in Figs. 3.10 (a) and 3.10 (b) respectively. The x-axis is the distance along the normal direction of the InGaN VCSEL. The insets of both figures are the magnified view of the electron and hole concentrations near the quantum wells. The right-hand side is the p-side. It is indicated from Fig. 3.10 (a) that the electron concentrations in the three quantum wells are approximately the same. However, the holes concentration in the quantum wells near the n-side are obviously lower than that near the p-side. These poor holes injection into the quantum wells near the n-side is owing to the small mobility and thermal velocity of the holes since the hole mass of the nitride materials are relatively large [17]. Figure 3.11 shows the diagram of the stimulated recombination rates at the same injection current level. The quantum wells near the n-side have lower stimulated recombination rates as expected. Finally, the wave intensity diagram at the same injection current level is

shown in Fig. 3.12. The x-axis is the distance along the radial direction and the y-axis is the distance along the normal direction of the InGaN VCSEL. The wave intensity is higher near the active layers as expected.

Figures 3.13 (a) and 3.13 (b) show the threshold current and current to light output conversion of VCSEL with different numbers of quantum wells. The threshold current of the diode with seven quantum wells is 25.8 mA. It is the lowest threshold current among these diodes. With the increasing of quantum well numbers, the threshold current will not decrease when the quantum well numbers is larger than seven.

Because the effective masses of holes are greater than that of electrons, the laser performance will not be better with the increase of quantum wells. The quantum wells near the n-cladding will not contribute to the radiative recombination. In Fig. 3.13 (b), with the increasing of numbers of quantum wells, the slop efficiency of the diode tends to decrease. Combining the results of Figs. 3.13 (a) and 3.13 (b), The VCSEL performance is best with seven quantum wells.

Figure 3.14 shows the laser output power as a function of current for the devices with variant n-type DBR diameter. The n-type DBR diameter is an important factor that controls the carrier density in the active layer. The device with larger n-type DBR diameter has lower carrier density because the current spreads more widely in space. This will increase the laser threshold current and reduce the slope efficiency. The reason of lower slope efficiency is that more percentage of photons in the active layer loosed for no upper reflect mirror.

Figure 3.15 shows that the power transformation of device with larger

diameter is higher than that of device with smaller diameter. Since smaller diameter device has lower threshold current, the energy transformation efficiency is higher than that of larger diameter device.

In order to have a better performance of the 440-nm VCSEL, we increase the number of p-DBR pair. From Fig. 3.6, the maximum reflectivity equals to 0.964 and 0.984 when the pair number is 30 and 40 respectively. Although it is hard to grow p-DBR, we designed a doable diode with 30 pairs p-DBR. As shown in Fig. 3.16, by introducing 40 pair p-DBR instead of 30 pair p-DBR, it will lower the threshold current to 9.2 mA.

Figures 3.17 (a) and 3.17 (b) show the threshold current and current to light output conversion of VCSEL with different numbers of quantum wells when the p-DBR pair increases to 40. The threshold current of the diode with four quantum wells is 7.2 mA. It is the lowest threshold current among these diodes with different quantum well numbers. With the increasing of quantum well numbers, the threshold current will not decrease when the quantum well numbers is larger than four.

Because the effective masses of holes are greater than that of electrons, the laser performance will not be better with the increase of quantum wells. The quantum wells near the n-cladding will not contribute to the radiative recombination. With the increasing of p-DBR pair, the total electric resistance increases, it will result in lower threshold current in four pair quantum well. In Fig. 3.17 (b), with the increasing of numbers of quantum wells, the slop efficiency of the diode tends to decrease when the quantum well number is larger than seven. Unfortunately, the result will not

support us to define that how many quantum wells is the best design.

Figure 3.18 shows the I-V curves of devices with variant numbers of quantum wells. The threshold voltage is a function of quantum well numbers. The quantum well number has large influence on the threshold current but just a little influence on the resistance. That is easy to be understood that most of the threshold voltage is used to overcome the undoped active region and spacer. The cavity length does not vary because the active region and the spacer have the same refractive indices; however, the more quantum wells induce more potential barriers. This results in higher threshold voltage. On the other hand, the thickness of the undoped region including active layer and spacer is very thin when compared to the total thickness of the device; therefore, the resistance caused by the potential barriers in the active region can be ignored.

For the consideration of power transformation, as shown in Fig. 3.19, four quantum wells is the best design. The slope efficiency of devices with four, six and eight quantum wells are almost equal, but the device with four quantum wells has the lowest threshold power and highest output power under equal electric input power. It is interesting to note that in Fig. 3.17 the device with ten quantum wells has lower threshold current and higher slope efficiency than the device with two quantum wells; however, they have almost equal threshold power although the device with ten quantum wells still has a higher slope efficiency.

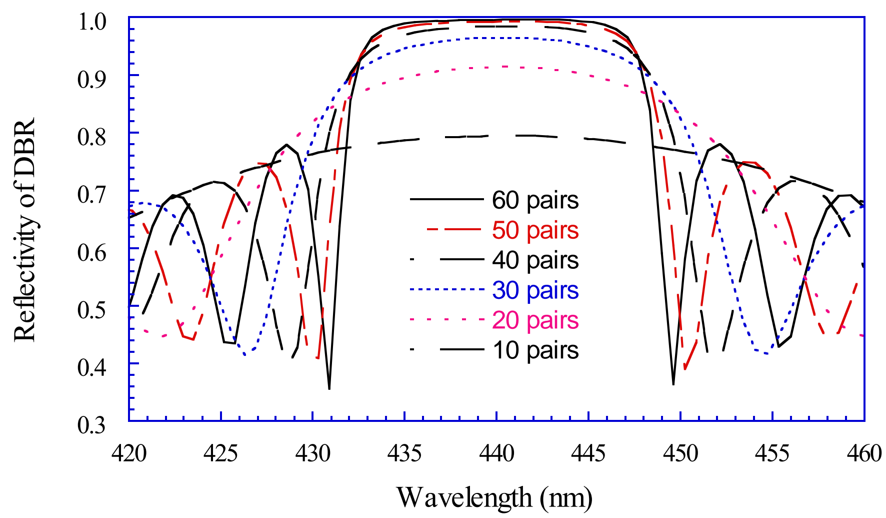

Fig. 3.6 Reflectivity spectra of the GaN/$Al_{0.27}Ga_{0.73}N$ DBR when the pair number of the DBR is equal to 10, 20, 30, 40, 50 and 60.

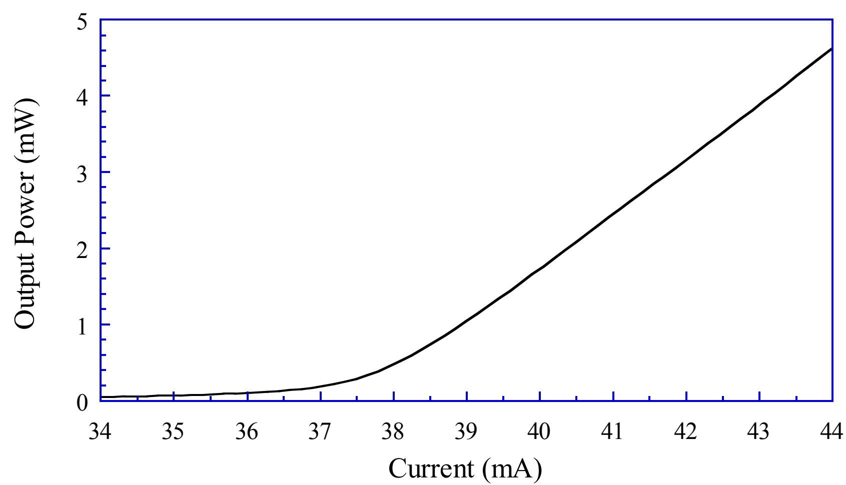

Fig. 3.7 L-I curve of the InGaN VCSEL under study at room temperature.

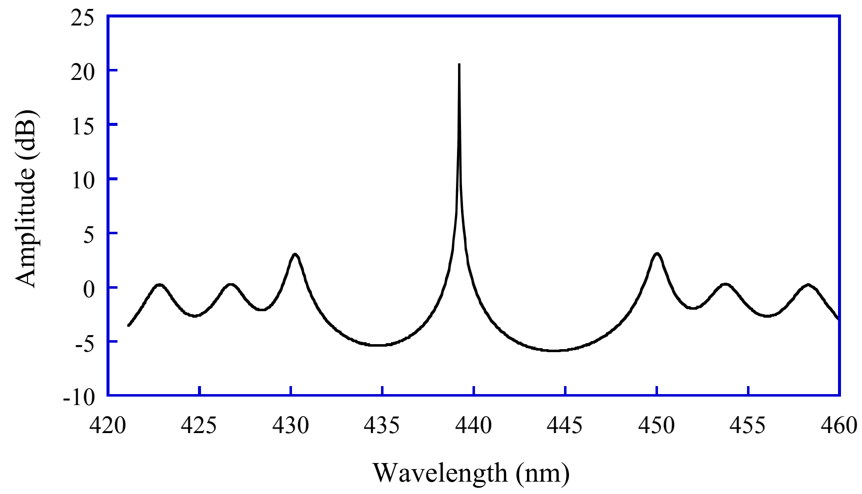

Fig. 3.8 (a) Mode spectrum when the injection current is at 33.9 mA.

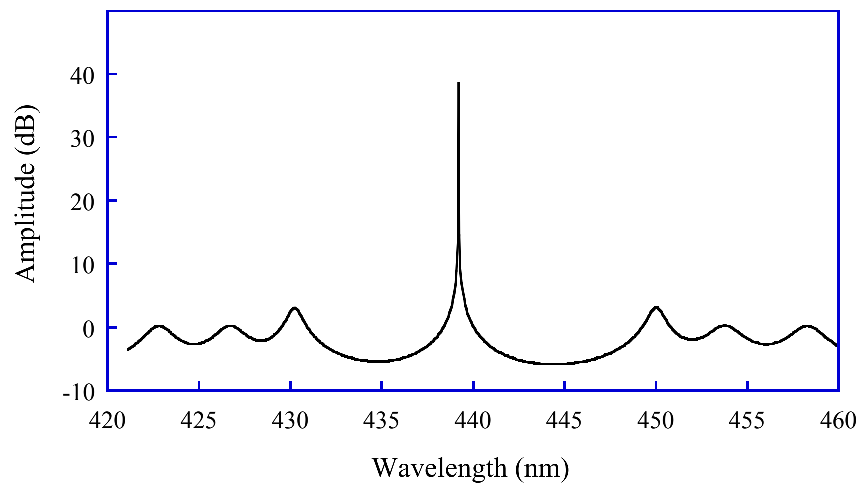

Fig. 3.8 (b) Mode spectrum when the injection current is at 41.4 mA.

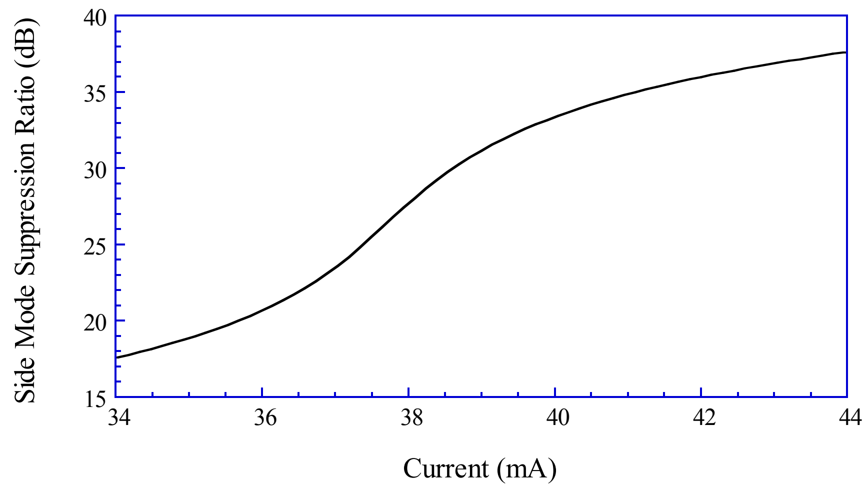

Fig. 3.9 Side mode suppression ratio as a function of the injection current.

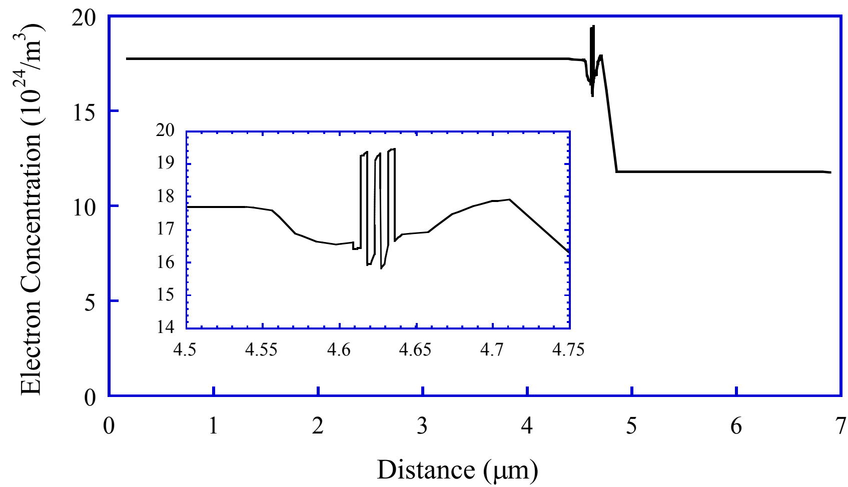

Fig. 3.10 (a) Distribution of the electron concentrations obtained at an injection current of 41.4 mA. The inset of figure is the magnified view of the electron concentrations near the MQW.

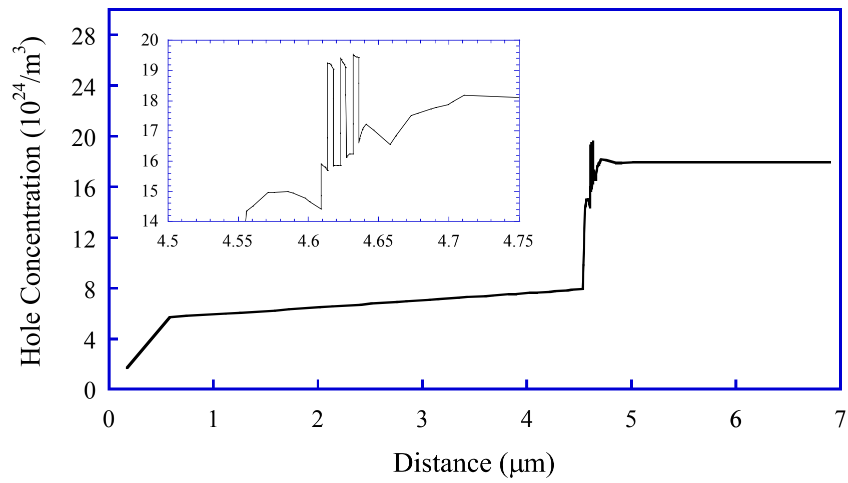

Fig. 3.10 (b) Distribution of the hole concentrations obtained at an injection current of 41.4 mA. The inset of figure is the magnified view of the hole concentrations near the MQW.

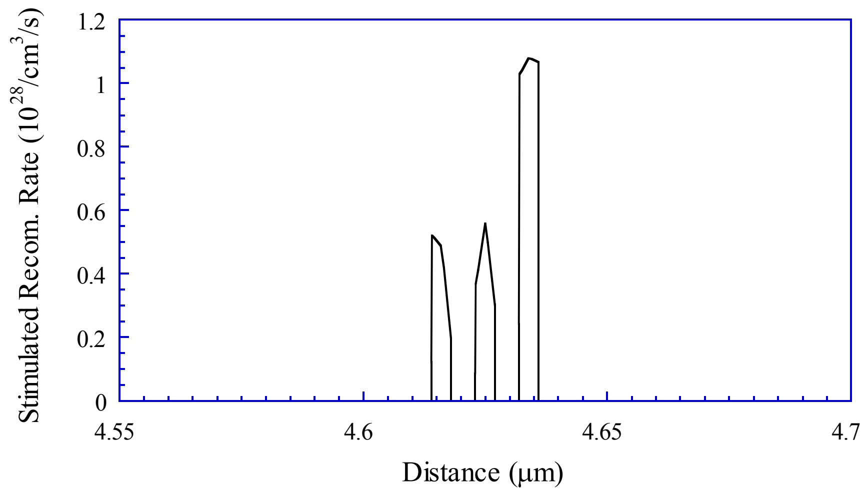

Fig. 3.11 Diagram of the stimulated recombination rates.

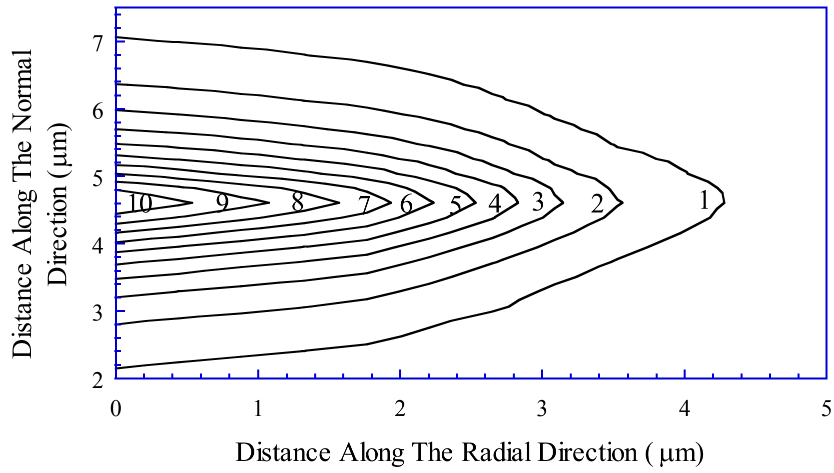

Fig. 3.12 Wave intensity diagram.

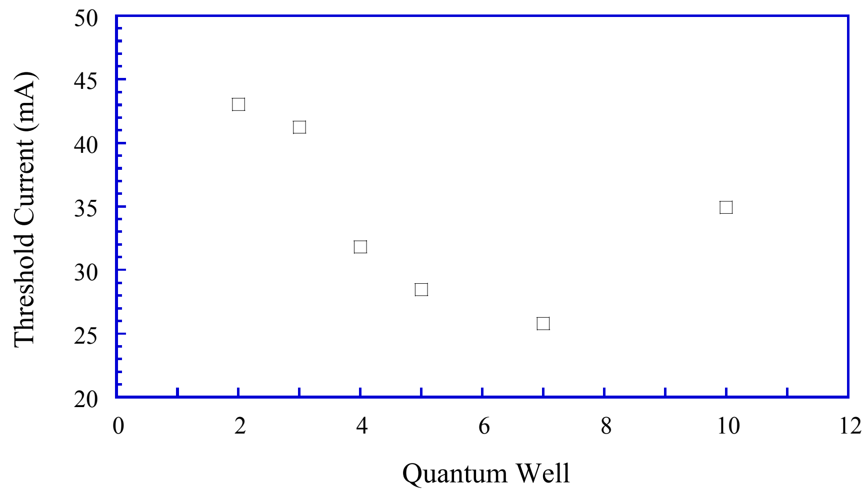

Fig. 3.13 (a) Threshold current with different numbers of quantum wells.

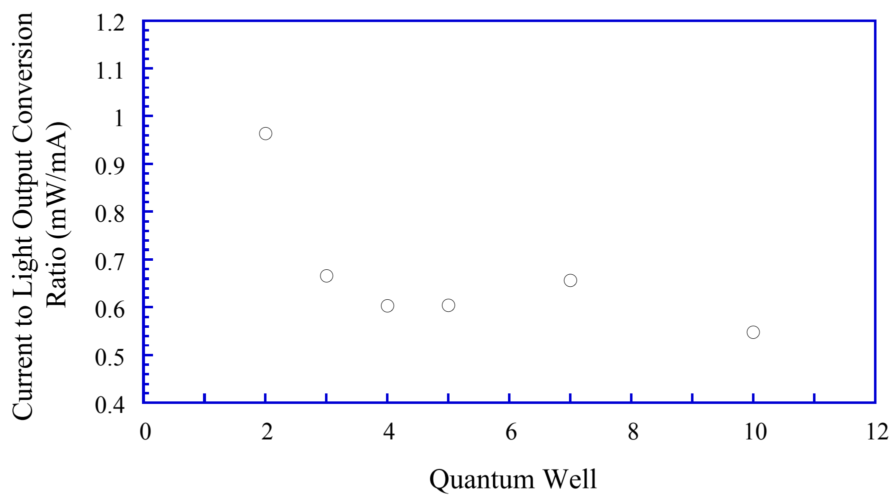

Fig. 3.13 (b) Current to light output conversion with different numbers of quantum wells.

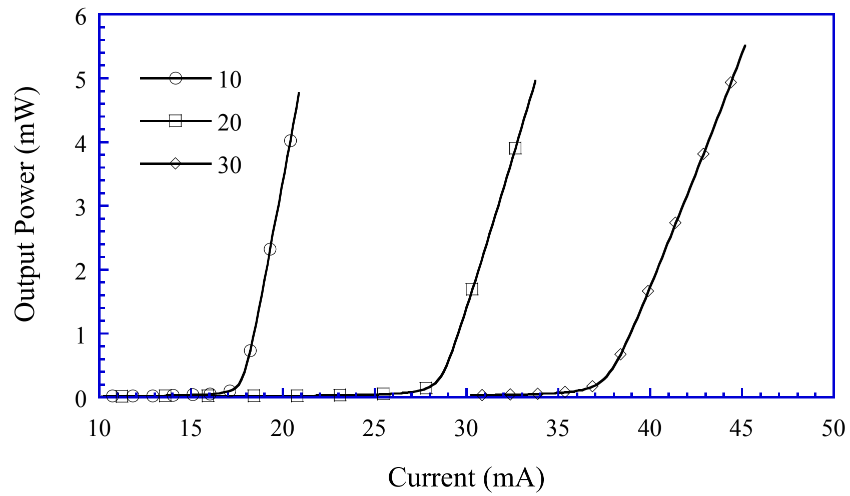

Fig. 3.14 Laser output power as a function of current for the devices with variant diameter.

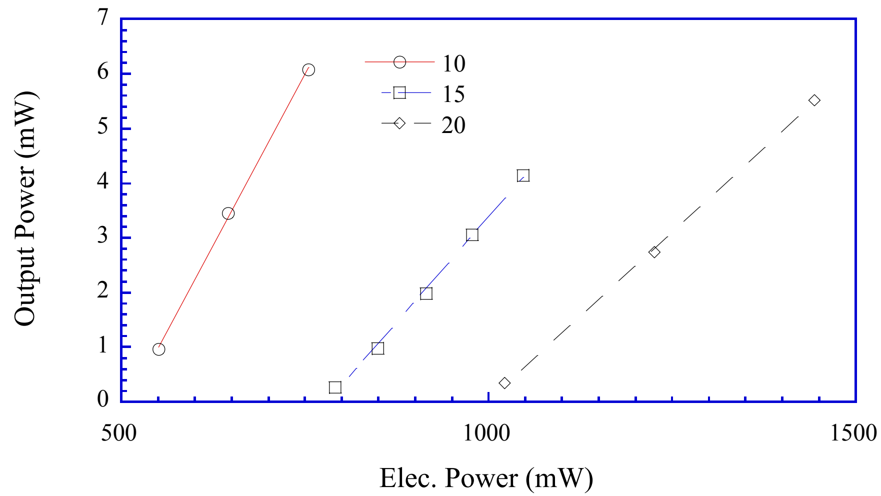

Fig. 3.15 Laser output power as functions of electric power with variance device diameters.

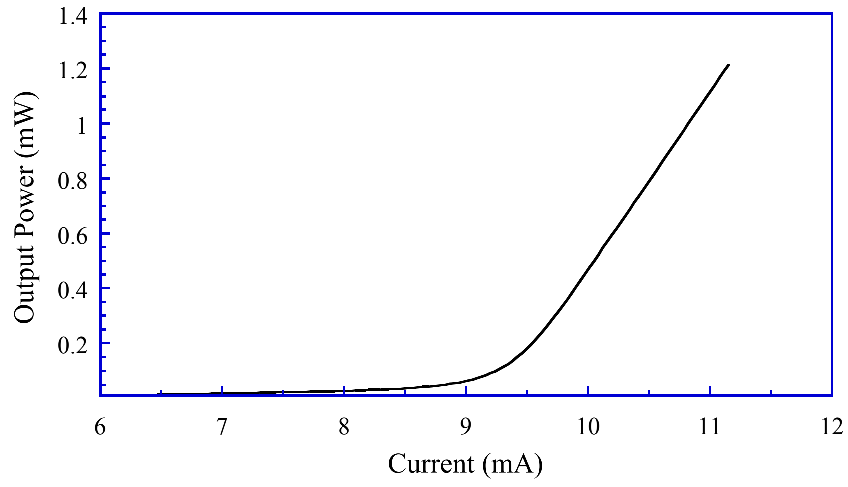

Fig. 3.16 L-I Curve of the InGaN VCSEL with 40-pairs of p-DBR under Study.

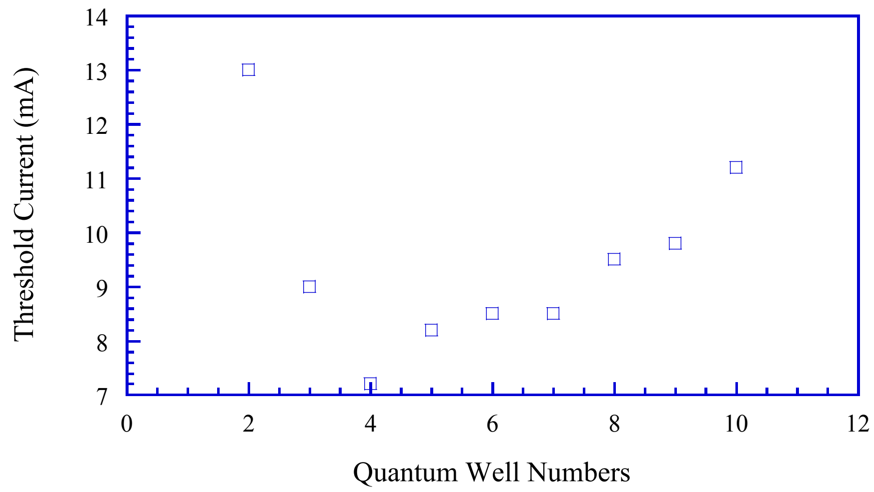

Fig. 3.17 (a) Threshold current with different numbers of quantum wells.

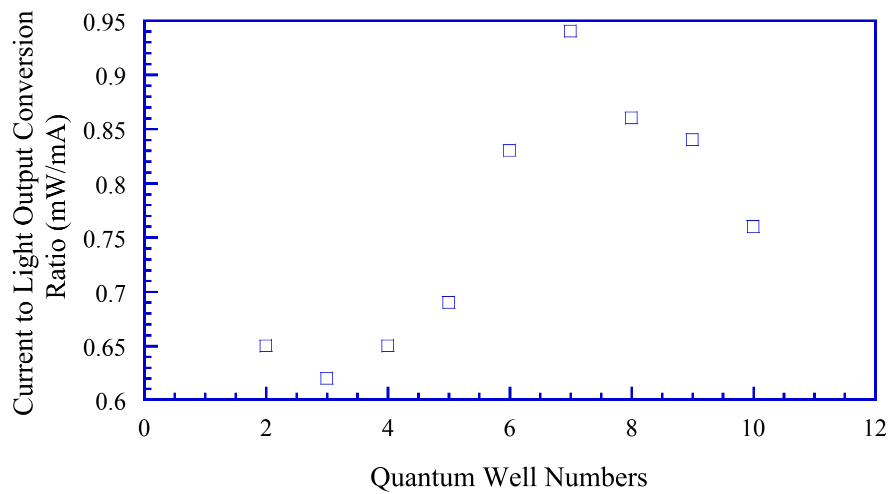

Fig. 3.17 (b) Current to light output conversion with different numbers of quantum wells.

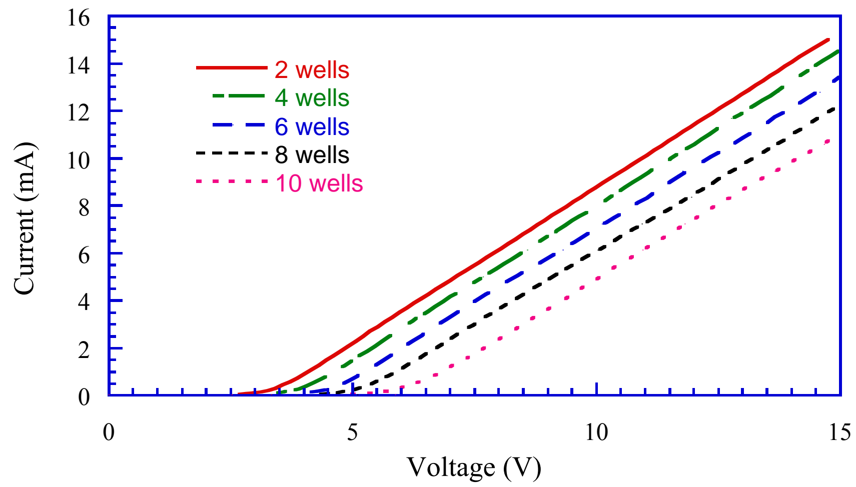

Fig. 3.18 I-V curves of devices with variant numbers of quantum wells.

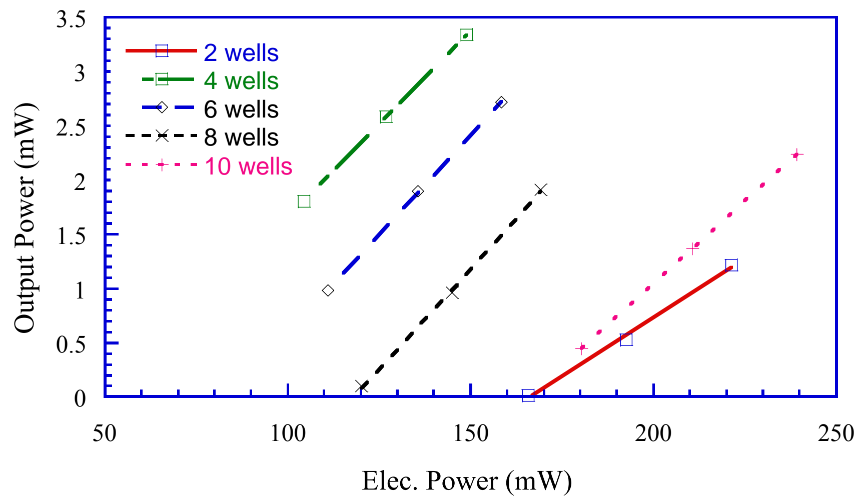

Fig. 3.19 Power transformation curves of the diode with variant numbers of quantum wells.

3.4 Discussion

In summary, the optical properties of an electrically pumped 440-nm InGaN MQW VCSEL are numerically investigated. The materials used for the DBR are GaN for the high-index layers and $Al_{0.27}Ga_{0.73}N$ for the low-index layers. The GaN/$Al_{0.27}Ga_{0.73}N$ DBR has a reflectivity of 99.3% for the high reflecting mirror (50 pairs) and 96.4% for the output coupling mirror (30 pairs) at the designed laser wavelength, 440 nm. The threshold current and slope efficiency of this blue InGaN VCSEL is 37.6 mA and 0.84 mW/mA, respectively. The side mode suppression ratio is 35.4 dB when the injection current is 10% above the laser threshold. Simulation results show that the electron concentrations in all the quantum wells are approximately the same while the hole concentrations in the wells near the n-side are lower than that near the p-side, which in turn results in a lower stimulated recombination rates in the quantum wells near the n-side. In addition, the best design of the structure is the use of seven pair of quantum wells. The quantum wells near the n-cladding will not contribute to the radiative recombination. In general, the performance of the diode with smaller diameter is better than that with larger one.

When the p-DBR pair increases to 40, the threshold current decreases obviously. For this kind of VCSEL, we have the lowest threshold current with four quantum wells and the maximum current to light output conversion ratio with seven quantum wells. With the increasing of quantum well numbers, the quantum well number has large influence on the threshold voltage but just a little influence on the resistance. In addition, if we take the power transformation into consideration, four quantum well

numbers is the best choice of active layer in designing 440-nm InGaN multi-quantum well VCSEL.

References

[1] S. Nakamura, "III-V nitride based light-emitting device," Solid State Comm., vol. 102, pp. 237-243, 1997.

[2] P. D. Floyd, C. L. Chua, D. W. Treat, and D. P. Bour, "Wafer fusion of infrared laser diodes to GaN light-emitting heterostructures," IEEE Photonics Tech. Lett., vol. 10, pp. 1539-1541, 1998.

[3] S. Nakamura, "InGaN-based blue light-emitting diodes and laser diodes," J. Cryst. Growth., vol. 202, pp. 290-295, 1999.

[4] S. C. Jain, M. Willander, J. Narayan, and R. Van Overstraeten, "III-nitride: Growth, characterization, and properties," J. Appl. Phys., vol. 87, pp. 965-1006, 2000.

[5] T. Shirasawa, N. Mochida, A. Inoue, T. Honda, T. Sakagucgi, F. Koyama, and K. Iga, "Interface control of GaN/AlGaN quantum well structures in MOVPE growth," J. Cryst. Growth., vol. 190, pp. 124-127, 1998.

[6] H. N. Ng and T. D. Moustakas,"High reflectance III-nitride Bragg reflectors grown by molecular beam epitaxy," MRS Internet J. Nitride Semicond. Res. 5, pp. NIL_28-NIL_32, 2000.

[7] H. Klausing, J. Aderhold, F. Fedler, D. Mistele, J. Stemmer, O. Semchinova, J. Graul, J. Danhardt, and S. Panzer,"Electron beam pumping in nitride vertical cavities with GaN/$Al_{0.25}Ga_{0.75}N$ Bragg reflectors," MRS Internet J. Nitride Semicond. Res. 5, pp. NIL_562-NIL_567, 2000.

[8] J. Han and M. H. Crawford, "Grwoth and characterization of AlGaInN for UV optoelectronics," Proc. IEEE Lasers and Electro-Optics Society 2000 Annual Meeting, vol. 2, pp. 557-558, 2000.

[9] PICS3D Manual Ver. 3.1 (Crosslight Software Inc., 1997)

[10] J. Piprek, P. Abraham, and J. E. Bowers, "Self-consistent analysis of high-temperature effects on strained-layer multiquantum-well InGaAsP-InP lasers," IEEE J. Quantu, Electron., vol. 36, pp. 366-374, 2000.

[11] N. Nakada, M. Nakaji, H. Ishikawa, T. Egawa, M. Umeno, and T. Jimbo, "Improved characteristics of InGaN multiple-quantum-well light-emitting diode by GaN/AlGaN distributed bragger reflector grown on sapphire," Appl. Phys. Lett., vol. 76, pp. 1804-1806, 2000.

[12] G. B. Stringfellow and M. Georage Craford, High Brightness Light Emitting Diodes - Semiconductors and Semimetals Volume 48, Academic Press, San Diego, California, USA, 1997.

[13] K. Osamura, S. Naka, and Y. Murakami, "Preparation and optical properties of $Ga_{1-x}In_xN$ thin films," J. Appl. Phys., vol. 46, pp. 3432-3441, 1975.

[14] G. P. Agrawal, Semiconductor Lasers, American Institute of Physics, Woodbury, New York, 1995.

[15] J. M. Redwing, D. A. S. Loeber, N. G. Anderson, M. A. Tischler, and J. S. Flynn, "An optically pumped GaN-AlGaN vertical cavity surface emitting laser," Appl. Phys. Lett., vol. 69, pp. 1-3, 1996.

[16] I. L. Krestnikov, W. V. Lundin, A. V. Sakharov, V. A. Semenov, A. S. Usikov, A. F. Tsatsul'nikov, Zh. I. Alferov, N. N. Ledentsov, A. Hoffmann, and D. Bimberg, "Room-temperature photopumped InGaN/GaN/AlGaN vertical-cavity surface-emitting laser," Appl. Phys. Lett., vol. 75, pp. 1192-1194, 1999.

[17] K. Domen, R. Soejima, A. Kuramata, and T. Tanahashi,"Electron overflow to the AlGaN p-cladding layer in InGaN/AlGaN MQW laser diodes," MRS Internet J. Nitride Semicond. Res. 3, 2 (1998).

Chapter 4. Conclusion

In the thesis, we simulated 670-nm AlGaInP based VCSEL with AlGaAs and AlGaInP DBR, respectively, and 440-nm InGaN based VCSEL with GaN/$Al_{0.27}Ga_{0.73}N$ DBR by PICS3D simulation program. For 670-nm AlGaInP based VCSEL, the results show that the reflectivity of AlGaAs DBR is higher than that of AlGaInP DBR having the same pair numbers and bandwidth of the AlGaAs DBR is wider, too. The laser performance of device with AlGaAs DBR is superior to that of device with AlGaInP DBR, for device with AlGaAs DBR has lower threshold current, higher slope efficiency and transformation efficiency from electric power to laser output power, and lower resistance. The threshold current raises with increasing device radiuses for at the threshold current, they have equal carrier density and population inversion density. However, the slope efficiency decreases with decreasing device radiuses. We can enhance the laser efficiency by utilizing gain-guiding structure.

For 440-nm InGaN based VCSEL with GaN/$Al_{0.27}Ga_{0.73}N$ DBR, the DBR reflectivity spectra of fifteen pairs we simulated is similar to that measured by N. Nakada *et al.,* GaN/$Al_{0.27}Ga_{0.73}N$ DBR has a reflectivity of 99.3% for the high reflecting mirror (50 pairs) and 96.4% for the output coupling mirror (30 pairs) at the designed laser wavelength, 440 nm. We can get laser output if the injection current is higher than 39.6 mA, and the slope efficiency of this blue InGaN VCSEL is 0.84 mW/mA. The stimulated recombination rate in quantum wells is not equal for the holes distribution is not uniform in the active region. The well nearest to the

p-space has the highest holes concentration and thus highest stimulated recombination rate. Similar to the 670-nm AlGaInP based VCSEL, the threshold current also increases with the effective cross-section in active layer, but the slope efficiency raises with the effective cross-section of active layer too, which is in contrast with that of 670-nm AlGaInP based VCSEL.

All the results can be taken as references when growing 670-nm AlGaInP based VCSEL and 440-nm InGaN based VCSEL.

To all the students in our group, we may investigate the further syntax of PICS3D and LASTIP. For the syntax we have known now, we can only simulate a simple diode structure. High technology and advanced study press us to higher state of research, such like thermal model, a diode close to reality, and so on. Let us try our best.

Appendix A
User guides of PICS3D

PICS3D is a set of software produced by Crosslight Software Inc. It can simulate semiconductor laser of about seven different structures and plot figures of about fifteen different types. Generally speaking, we can divide the production of semiconductor into growing of films and production of diodes. When we talk about the growing of films, we can use *.gain to describe it; by the same token, we need to depict the production of diodes is a whole procedures. And we will describe the details as follows:

(i) *.layer

This file consists of high-level language of the most outside's program by which we use it to describe the structure of diode. We usually cooperate it with *.bar and *.well which represents respectively materials of barriers and wells.

We use "column" to decide the width of the diode, the thickness of each layer to decide the height (layer d=). Moreover, we need to cooperate it with the coating location of "bottom_contact" and "top_contact" (column_num= from= to=), and so the whole outside structure of cylindrical diode is formed.

And then, we need to define each of the layered structures. We usually call the material of non-active region "bulk macro", and the active region the "active macro." We need to think it over that how can we make the definition of a "bulk" layer. It, of course, is conclusive of "section_loss=",

“section_index=”, and “macro_name=” and we cooperate it with doping concentration and material thickness, and so we succeed in defining the “spacer”. However, we must pay attention to the “macro_name” we decide to pick up when we write down the material. And the number of “var” is needed to be cooperated with the designing of “crosslight.macro” and your own designing.

In the process of designing a VCSEL, DBR is the most important part to which we need to pay attention to. The syntax of DBR is the same as “bulk”, and we can view each pair of DBR as an averaged material. That is, we first add these two layers of parameter, divide them, secondly, define the thickness and refractive index of these two respectively, and finally cooperate it with the syntax of “bulk”, and so the whole structure of DBR is formed then. And then, there is only the active region left. It is consisted of two parts, barrier and well. We usually write down another two files (*.bar and *.well.) The “*.bar” define barrier and the syntax is the same as bulk. The *.well represent well, but we need to get it changed to “active macro” in the part of macro. The only one thing we need to pay attention to here is to decide it in accordance with the macro(crosslight.macro).

After we finish the layer part, we make a movement of process layer (c:\crosslig\pics3d\pics3d.exe *.layer), the program will turn the interior into the low-layered language. And the five files *.mater, *.doping, *.geo, *.mplt, and *. vcsel define respectively materials and characters, doping concentration, geometrical structures and mesh numbers, the controlling file of plotting the mesh line, and the definition of VCSEL’s different areas. These several files completely describe each of the details of a designed

VCSEL by which we use to simulate.

(ii) *.gain

The so-called *gain, we can take it as film growing. In LASTIP (LASerTechnology Integrated Program) simulation, *.gain independent to the whole procedure for edge emitting laser. It defines the material width of the film and electron transition lifetime. By setting all the parameter, we can understand the characteristics of the film after acting “process .gain file”. That is emitting wavelenth, strain effect, and so on. It will provide us the information for predicting the result of growing the films in the active region of a diode. In PICS3D simulation, *.gain become a part in final simulation. I order that we have *.mater after processing layer, it contains all the parameter of the active region.

PICS3D will attach all the parameters at the *.mater (include file=*.mater). In general, the electron transition lifetime is usually defined as one pico second. In PICS3D simulation, we got to edit the carrier concentration, wavelength region, and figure types.

(iii) *.sol

The so-called *.sol means solution. Briefly speaking, we start to simulation a real diode with current injection now. For a VCSEL, we got to know the characteristics of DBR first, including reflection coefficient and types of standing wave. And then, we can know the characteristics of a VCSEL finally. Therefore, we divide the simulation process into two parts,

characteristics of DBR and diode after current injection. These two procedures are separated by the statement “stop”.

In *.sol, we got to define the refractive index inside and outside the cylinder first. And then, we define the background loss, estimated peak wavelength, and wavelength region. After we define the value of rtgain_phase density, we set a statement “stop”. The “run existing .sol file” process will stop here and we complete the first stage of simulation. With the use of *.rtgain, we can plot the figure of reflection coefficient and standing wave in DBR predicting. However, all the text data are all saved as *.rtd and *.stw.

After completing the previous process, if the DBR was able to be used for a VCSEL, we can proceed into second stage of the simulation. In PICS3D simulation, we got to predict the transparency current first. After injecting current, as long as the model gain peak reach 10^5 (1/m), it represent the transparency current. Therefore, we predict the transparency current by injecting higher current value. That is, we add a statement “stop” in back of the region where we define current injection in *.sol file. During the procedure, we can find the situation of transparency current in *.log file. That is, we complete the second stage of simulation.

The final simulation is controlled by a statement “scan3d”. It define current injection range of a VCSEL for intact simulation. However, we must pay attention that the starting value of current which can not be larger than threshold current.

(iv) *plt

After all the procedure of simulates a diode, PICS3D will save the data in many files. Unfortunately, it can not be understood and read, but it will output by cooperating *.plt" file. The output file contains many kinds of styles. We often measured it by postscript and text file. We can choose the data point in *.log file to plot which the figures we want. After "view result (*.plt), we complete all the procedures of PICS3D simulation. Of course, there are some bugs during the total simulation, we will discuss in appendix B.

Appendix B
Trouble Shooting

PICS3D and LASTIP were originally working on UNIX operating system. Because the UNIX is not familiar to us, PICS3D and LASTIP were transplanted into Microsoft disk operating system (MSDOS) by Crosslight Software Inc. Therefore, it will cause some problem in using of the software. If it was clipped in any segment, it will cost you so much time for solving. I will try my best to describe each of detail problems blow:

(i) *.layer

In MSDOS, the width is eighty bytes in each line. If the sentences are longer than 80 bytes, it will add on next line automatically. What can I do if I have a long line of statements and I got to add on the file execute on MSDOS?

The software designer add a statement "&&". We can connect two or three lines by adding "&&" on each ends of lines. In the centuries of windows95, some editors of text file, i.e. notepad, it had already supported to 256 bytes in each lines. It will not be cut when it reaches 80 bytes automatically. And then, the line lost.

In fact, we can solve it by "EDIT.EXE" in MSDOS prompt to identify where to add "&&". As shown above, it usually happened when we edit ".layer" file. If some problems occurred, you can check the ".layer" file first. Although it may be a piece of cake, it will lead to the great chain-reaction.

(ii) *.gain

In generating *.gain, it often get trouble on the problem of carrier concentration. But it will take place when we run *.sol file. We got to set the same carrier concentration in each figure.

By the way, we can plot the figure with different carrier concentration, but we got to run *.gain with the same carrier concentration in each files finally. It will not be any more problem when we run *.sol.

Besides, the syntax of *.gain in PICS3D is the same with that of in LASTIP. If we are familiar to the syntax of LASTIP, we can run the *.gain by the file of LASTIP. However, we must pat attention that the *.gain file of LASTIP is just for predicting the properties of thin film. We got to use the syntax of PICS3D, when the thin films are taken as the active region of a real diode.

(iii) *.sol

In generating *.sol file, the system will occur a resident pattern “ppmon”. It will not be stopped after we finished the simulation of a diode. When we run the next *.sol, it will output a *.log file. And then, it will occur a problem “File Creation “Error”.

By the way, we have to press “ctrl+alt+del” to close the resident pattern “ppmon” to have the file been executed continuously. Besides, there will not be any problem in *.sol file. However, if we got some problem in running previous file, it will make mistakes in running *.sol. How could we

solve the problem? Experience talks.

(iv) *.plt

There are some problems in setting “data_set”. If the “3d_data” and “3d_log” will not reach the available files, it will result problems in plotting figures.